



Geochemical and geochronological records of tectonic changes along a flat-slab arc-transform junction: Circa 30 Ma to ca. 19 Ma Sonya Creek volcanic field, Wrangell Arc, Alaska

Samuel E. Berkelhammer¹, Matthew E. Brueseke¹, Jeffrey A. Benowitz², Jeffrey M. Trop³, Kailyn Davis², Paul W. Layer², and Maridee Weber¹

¹Department of Geology, Kansas State University, 108 Thompson Hall, Manhattan, Kansas 66506, USA

²Geophysical Institute and Geochronology Laboratory, University of Alaska Fairbanks, Fairbanks, Alaska 99775, USA

³Department of Geology & Environmental Sciences, Bucknell University, Lewisburg, Pennsylvania 17837, USA

■ ABSTRACT

The Sonya Creek volcanic field (SCVF) contains the oldest in situ volcanic products in the ca. 30 Ma–modern Wrangell Arc (WA) in south-central Alaska, which commenced due to Yakutat microplate subduction initiation. The WA occurs within a transition zone between Aleutian subduction to the west and dextral strike-slip tectonics along the Queen Charlotte–Fairweather and Denali–Duke River fault systems to the east. New ⁴⁰Ar/³⁹Ar geochronology of bedrock shows that SCVF magmatism occurred from ca. 30–19 Ma. New field mapping, physical volcanology, and major- and trace-element geochemistry, coupled with the ⁴⁰Ar/³⁹Ar ages and prior reconnaissance work, allows for the reconstruction of SCVF magmatic evolution. Initial SCVF magmatism that commenced at ca. 30 Ma records hydrous, subduction-related, calc-alkaline magmatism and also an adakite-like component that we interpret to represent slab-edge melting of the Yakutat slab. A minor westward shift of volcanism within the SCVF at ca. 25 Ma was accompanied by continued subduction-related magmatism without the adakite-like component (i.e., mantle-wedge melting), represented by ca. 25–20 Ma basaltic-andesite to dacite domes and associated diorites. These eruptions were coeval with another westward shift to anhydrous, transitional-tholeiitic, basaltic-andesite to rhyolite lavas and tuffs of the ca. 23–19 Ma Sonya Creek shield volcano; we attribute these eruptions to intra-arc extension. SCVF activity was also marked by a small southward shift in volcanism at ca. 21 Ma, characterized by hydrous calc-alkaline lavas. SCVF geochemical compositions closely overlap those from the <13 Ma WA, and no alkaline lavas that characterize the ca. 18–10 Ma eastern Wrangell volcanic belt exposed in Yukon Territory are observed. Calc-alkaline, transitional-tholeiitic, and adakite-like SCVF volcanism from ca. 30–19 Ma reflects subduction of oceanic lithosphere of the Yakutat microplate beneath North America. We suggest that the increase in magmatic flux and adakitic eruptions at ca. 25 Ma, align with a recently documented change in Pacific plate direction and velocity at this time and regional deformation events in southern Alaska. By ca. 18 Ma, SCVF activity ceased, and the locus of WA magmatism shifted to the south and east. The change in relative plate motions would be expected to transfer stress to strike-slip faults above the inboard margin of the subducting

Yakutat slab, a scenario consistent with increased transtensional-related melting recorded by the ca. 23–19 Ma transitional-tholeiitic Sonya Creek shield volcano between the Denali and Totschunda faults. Moreover, we infer the Totschunda fault accommodated more than ~85 km of horizontal offset since ca. 18 Ma, based on reconstructing the initial alignment of the early WA (i.e., 30–18 Ma SCVF) and temporally and chemically similar intrusions that crop out to the west on the opposite side of the Totschunda fault. Our results from the SCVF quantify spatial-temporal changes in deformation and magmatism that may typify arc-transform junctions over similar time scales (>10 m.y.).

■ INTRODUCTION

Volcanic arcs have long been recognized as locations of continental crust formation and are a key component of subduction. The geochemistry and temporal-spatial distribution of lavas erupted from arc volcanic centers located above a subduction zone depend on many factors involving the nature and geometry of the subducting and overriding plates (Stern, 2002). The position, rate and angle of convergence, and dip of the actively subducting slab can determine the physical conditions under which source melting and eruption can occur (Syracuse and Abers, 2006; Portnyagin and Manea, 2008; England and Katz, 2010; Grove et al., 2012).

Along with “typical” calc-alkaline magmas that are a result of hydrous melting of the mantle wedge, the subducted oceanic plate itself can undergo partial melting. There are many conditions and contributing factors under which melting can be triggered including sediment influx at the trench, fluids fluxed off the slab, composition of the upper plate, angle, rate, and geometry of subduction (Cross and Pilger, 1982; Pearce and Peate, 1995; Borg et al., 1997; Castillo, 2012; Stern, 2002; Kelemen et al., 2003; Pearce et al., 2005). These settings also influence volcanic product geochemistry. Similarly, translation of the upper plate along strike-slip faults can play a role on the conditions under which melting and magma evolution can occur (Cole and Basu, 1992, 1995).

Detailed study of long-lived, well-preserved volcanic arc types and their eruptive products can help better illuminate these competing phenomena

and how they influence arc geochemistry. Arc-transform boundaries comprise an underappreciated type of subduction zone configuration (Park et al., 2002). These arc-transform junctions are found across Earth (e.g., Kamchatka, Central America, etc.) and document both upper- and lower-plate translation. The geochemistry of arc-transform volcanic products is affected by both the underlying plate geometry and the composition and structural configuration of the upper plate. Net extensional forces across a strike-slip fault (i.e., transtension) can trigger decompression melting, and lateral motion along the fault may translate a volcanic center significant distances from its original position (Cole, 1990; Vaughan and Scarrow, 2003; Bai and Montési, 2015). However, only a few studies have carefully documented variations in the geochemistry and physical volcanology of volcanic fields constructed along such plate margin transition zones (notable exceptions include Park et al., 2002; Maury et al., 2004; Portnyagin et al., 2005; Tibaldi et al., 2010; Lee et al., 2016).

Moreover, arc-transform magmatic junctions may involve flat-slab subduction. Flat-slab subduction occurs over 10% of the modern convergent margins (Gutscher et al., 2000). Flat-slab volcanic products are understudied because flat slabs often lead to the near total cessation of arc magmatism, yet the edge of the flat slab can generate significant arc magmatism (Portnyagin et al., 2005). The ca. 30 Ma to present Wrangell Arc (WA) of south-central Alaska (Richter et al., 1990; Preece and Hart, 2004; Trop et al., 2012; Brueseke et al., 2019) is a classic example of an arc-transform subduction configuration along the edge of a flat slab, hence an ideal location to study the geochemical signatures of flat-slab subduction and transtension in an arc-transform setting.

This study presents new data on the physical, spatial, and temporal characteristics of a largely unstudied volcanic field within the subduction-dominated, Alaskan portion of the Wrangell volcanic belt (WVB; i.e., the Wrangell Arc [WA]; Brueseke et al., 2019) in south-central Alaska. This volcanic field was chosen because it was apparently active at the initiation of the arc based on reconnaissance geochronological data (Richter et al., 1990). The primary objective of this paper is to evaluate the geochemical, geochronological, and stratigraphic characteristics of the volcanic and shallow intrusive rocks of the WA Sonya Creek volcanic field (SCVF), with the goal of constraining their petrogenetic processes and tectonic setting in which they originated. The secondary objective is to use the SCVF as an analog for the geological signatures during arc initiation in an arc-transform junction.

■ GEOLOGICAL BACKGROUND

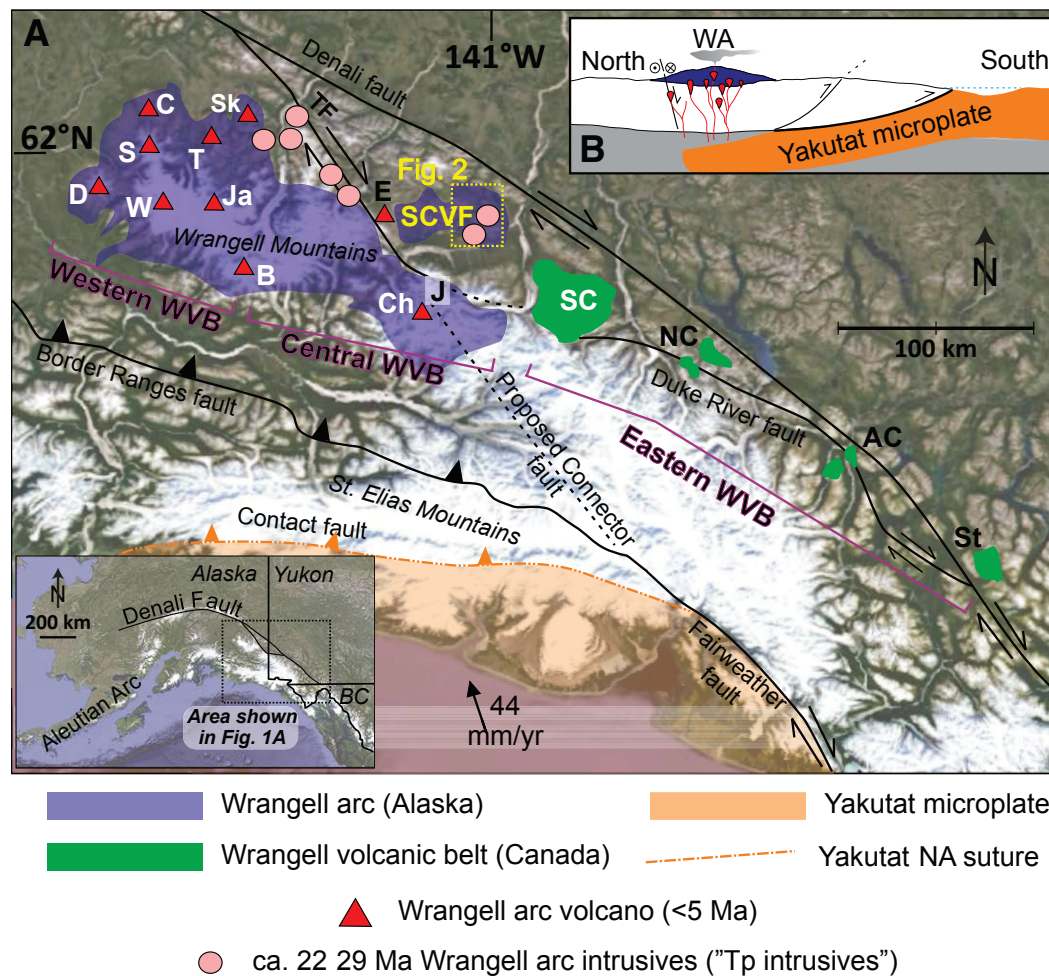
The northeastern Pacific plate margin is presently characterized by northwestward convergence along the southern Alaskan margin and shows a west to east transition from typical subduction to flat-slab subduction to strike-slip tectonics (e.g., Eberhart-Phillips et al., 2006; Haeussler, 2008). Subduction of the Yakutat microplate, interpreted to be anomalously thick and buoyant oceanic crust (e.g., an oceanic plateau), is responsible for Oligocene–Holocene volcanism and deformation in eastern Alaska (Plafker and Berg, 1994;

Pavlis et al., 2004; Benowitz et al., 2011, 2014, 2019; Worthington et al., 2012). Recent geophysical studies beneath south-central Alaska reveal an eastward increase in the angle of the subducted Yakutat slab, from ~6° south of the Talkeetna Mountains, and ~11° to 16° below the volcanoes of the Wrangell Mountains, with a projected depth of 80 km to the top of the slab (Bauer et al., 2014; Pavlis et al., 2019). Geophysical studies by Martin-Short et al. (2018) and Venereau et al. (2019) suggest that modern WA volcanism occurs along the eastern edge of Yakutat slab, due to mantle upwelling and melting along the slab edge. Brueseke et al. (2019) suggest that the WA has been at the leading edge of the slab since ca. 30 Ma; implicit in their study is that slab-derived components, fluxed off the subducting Yakutat slab, played a key role in WA igneous geochemistry.

Above the flat-slab region west of ~148°W, the upper plate exhibits limited volcanism due to crustal stresses that inhibited the rise and eruption of magmas generated from heating and dehydration of the subducted slab (e.g., McNamara and Pasyanos, 2002; Nye et al., 2002; Finzel et al., 2011). Subduction of oceanic lithosphere with thick crust (aseismic ridges, oceanic plateaus, or seamount chains) often coincides spatially and temporally with the absence of arc volcanism (e.g., McGeary et al., 1985; van Hunen et al., 2002). Small-volume eruptions of magmas have been emplaced locally along the leading edge of the Yakutat flat slab, far inland from the subduction zone. For example, spatially limited Holocene maars along the north flank of the Alaska Range record magma eruptions ~500 km inboard of the trench (Nye et al., 2002).

The eastern region of the tectonic transition zone (east of ~148°W) displays active volcanism in the WA, shallow seismicity, and displacement along the Denali–Duke River–Totschunda and Queen Charlotte–Fairweather right-lateral strike-slip fault systems (Fig. 1; Page et al., 1991; Eberhart-Phillips et al., 2003; Preece and Hart, 2004; Qi et al., 2007; Haeussler et al., 2017). The entire Denali–Duke River–Totschunda fault system comprises a northward extension of right-lateral transform motion between the Pacific plate and Yakutat microplate past the North American continent along the Queen Charlotte–Fairweather fault systems (Kalbas et al., 2008). A possible connecting fault that links the Totschunda and Fairweather may strike to the southeast between the two faults (e.g., Connector fault on Fig. 1; Richter and Matson, 1971; Kalbas et al., 2008). Aberrations from pure strike-slip motion along this complex system result in localized areas that show components of transtensional and transpressional basin development along the Duke River fault (Ridgway and DeCelles, 1993).

The WA is located within this eastern region of tectonic transition zone overlying the Wrangellia composite terrane. The Wrangellia composite terrane is composed of Paleozoic to Precambrian continental margin rocks, a Triassic oceanic plateau (e.g., Nikolai Formation), and Jurassic–Cretaceous island arcs (Nokleberg et al., 1994; Greene et al., 2008). We acknowledge that this long prior history of magmatism has likely affected the pre–30 Ma lithospheric mantle below the study area. Previous geochemical studies of ca. 30–0.1 Ma igneous rocks show that the processes of subduction, slab melting, and motion along strike-slip faults have all contributed to magma geochemistry



at distinct volcanic centers during the lifetime of the arc (Nye, 1983; Richter et al., 1990; Skulski et al., 1991, 1992; Preece and Hart, 2004; Trop et al., 2012; Brueseke et al., 2019).

In the western WA, Preece and Hart (2004) documented three geochemical trends and/or suites in <5 Ma volcanic rocks in the western WA (trend 1—transitional-tholeiitic; trend 2a—"typical" subduction-related calc-alkaline; trend 2b, adakite) and described the geochemical significance of each trend in three geographic zones: front-side, interior, and back-side volcanoes (Figs. 1 and 2). Less than 5 Ma eruptive products are from large composite shield volcanoes (Mounts Blackburn, Jarvis, and Sanford; Tanada Peak; Capital

Mountain; and Skookum Creek volcanic complex), stratovolcanoes (Mounts Drum and Churchill), and a series of aligned cinder cones in the interior of the western WA. Preece and Hart (2004) suggest that Trend 1 rocks (dominantly from the interior of the WA) represent relatively low degrees of melting due to localized intra-arc extension, resulting in fast magma ascent rates and minimal fractional crystallization. Trend 2a rocks constitute the largest volume of <5 Ma WA volcanic products and show "typical" subduction-related calc-alkaline geochemical affinities that suggest somewhat higher degrees of partial melting due to fluid flux into the mantle wedge (Preece and Hart, 2004). Trend 2b rocks occur only on the front side of the modern WA, and their

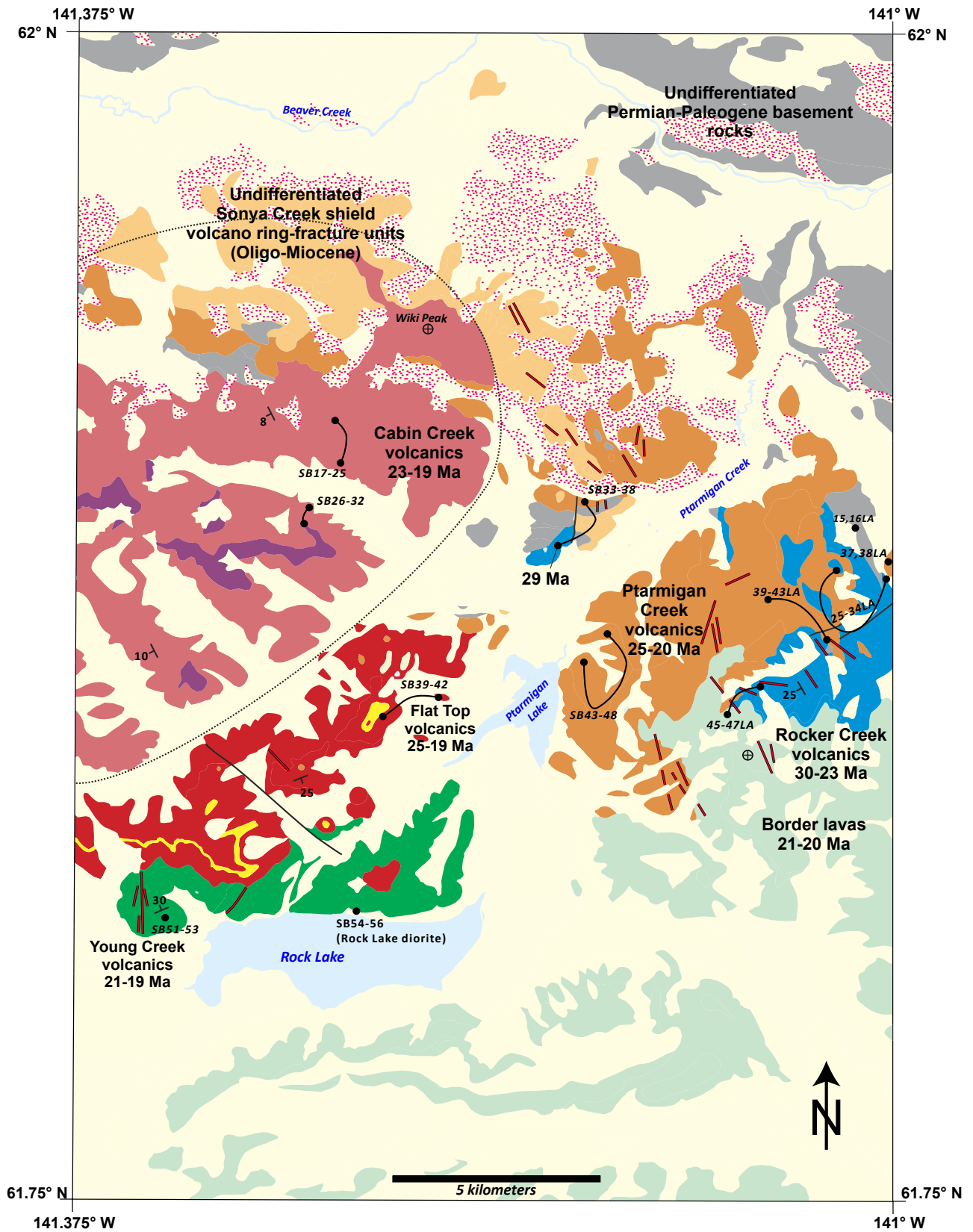
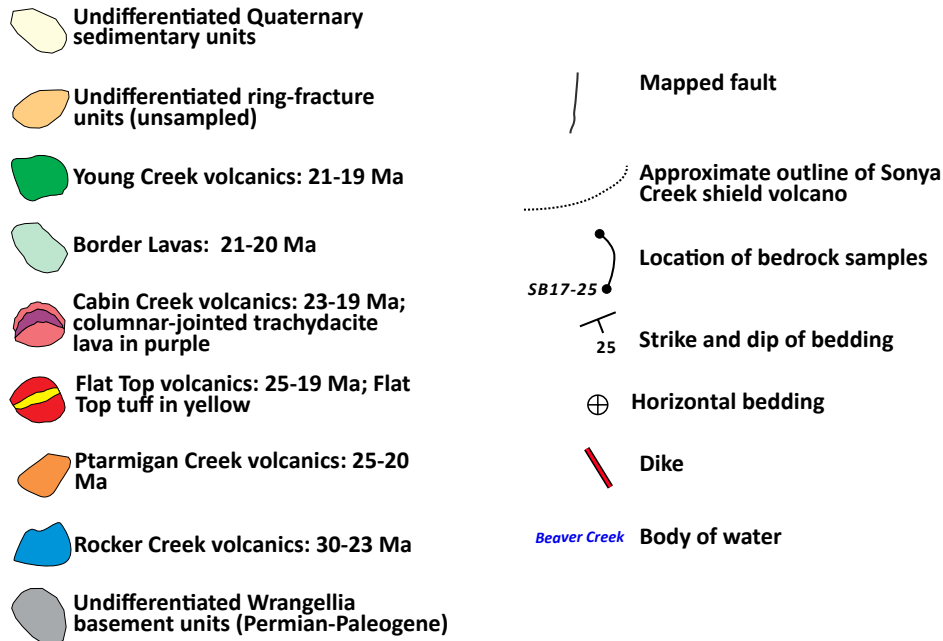


Figure 2 (continued on following page). Geologic map of the Sonya Creek volcanic field (SCVF) simplified from Richter et al. (2000) and our new geochemical constraints. Refer to Figure 1 for map location. Black circles with lines mark locations of geochronological and/or geochemical bedrock samples for the present study. Samples beginning with “SB” follow the SB15-xx numbering scheme, and samples ending with “LA” follow the 15JBxxLA scheme. Bedrock units are combined into geographic units described in the text and legend (e.g., Flat Top volcanics).

Map Units and Symbols



This Study	Richter et al. (2000)
Undifferentiated ring-fracture units (unsampled)	Sonya Creek shield volcano (Tsu; Tm; Tcc; Tsb; Tsf; Tsp; Tsd)
Young Creek volcanics: 21-19 Ma	Young Creek volcanic and volcanoclastic rocks (Tol- ca. 19 Ma K-Ar ages) and Tdd diorite (Rock Creek diorite)
Border Lavas: 21-20 Ma	Border volcanic and volcanoclastic rocks (Tbpa; Tba; Tbl)
Cabin Creek volcanics: 23-19 Ma; columnar-jointed trachydacite lava in purple	Sonya Creek shield volcano (Twi, Lavas of Wiki Peak are main volume - 20 Ma K-Ar age; Twr, columnar-jointed trachydacite lava; Trt, Tp, Tbc, Tpf, Tm, Tvu)
Flat Top volcanics: 25-19 Ma; Flat Top tuff in yellow	Sonya Creek shield volcano shield rocks (Tsa, Flat Top tuff; Tsm, Tsl)
Ptarmigan Creek volcanics: 25-20 Ma	Dacite dome field and associated subvolcanic rocks (Tdh - 23 Ma K-Ar age; Tdr; Tdqd, Tr)
Rocker Creek volcanics: 30-23 Ma	Rocker Creek volcanic and volcanoclastic rocks (Trr; Trp; Trl - 26 Ma K-Ar age)

Figure 2 (continued).

adakitic character is attributed to partial melting of the Yakutat slab (Preece and Hart, 2004; Preece et al., 2014).

In the central WA (Fig. 1), Trop et al. (2012) showed that trends 1 and 2a erupted from ca. 12–5 Ma into intra-arc basins, but trend 2b volcanic products are not recognized there. Trop et al. (2012) also documented north-trending Miocene faults and dikes, consistent with transtension from the northwest-trending Totschunda fault, in the central WA. Trop et al. (2012) concluded that the same types of magma generation processes (e.g., mantle-wedge melting due to subduction and low-degree melting of mantle less affected by subduction due to intra-arc extension) that characterized the <5 Ma western WA, affected the central WA during Miocene time. Trop et al. (2012) focused on part of the southern portion of the central WA. The northern part of the central WA was essentially unexplored (until the present study) except for a handful of geochronological and geochemical analyses completed as part of regional geological mapping studies (Richter 1976; Richter et al., 2000). More recent work from the central WA (Brueseke et al., 2019) has demonstrated that since initiation at ca. 30 Ma to the present, the Wrangell volcanic belt in Alaska has been an arc, continuously producing volcanic products with a subduction signature (trend 2a). Additionally, Brueseke et al. (2019), concluded slab-edge upwelling, flat-slab defocused fluid flux, and faults acting as magma conduits are likely responsible for the exceptionally large volcanoes and high eruption rates of the Wrangell Arc.

The eastern WA in southwestern Yukon Territory and northwestern British Columbia, Canada, is characterized by a series of northwest-southeast-trending volcanic fields and records WA volcanism along the Duke River strike-slip fault (Fig. 1A; Skulski et al., 1991, 1992). The Stanley Creek volcanic field, the smallest of these fields and the farthest to the southeast, is composed of undated transitional and minor alkaline lavas (St on Fig. 1A; Skulski et al., 1991). The Alsek field is composed of ca. 14–11 Ma calc-alkaline and volumetrically minor transitional and alkaline lavas (AC on Fig. 1A), and the Nines Creek field consists of ca. 16–13 Ma transitional lavas (NC on Fig. 1A; Dodds and Campbell, 1988). The St. Clare Creek field is adjacent to the Yukon-Alaska border and comprises ca. 18–10 Ma transitional and minor alkaline and calc-alkaline lavas (SC on Fig. 1A; Skulski et al., 1992). The St. Clare Creek volcanic field contains two distinct and overlapping composite volcanoes, termed the Wolverine and Klutlan eruptive centers. The ca. 18–16 Ma Wolverine center shows a chemo-stratigraphic trend from >17.8 Ma alkaline basalts at the base to transitional lavas in the middle of the section, to ca. 16 Ma calc-alkaline lavas at the top of the succession. The ca. 16–10 Ma Klutlan center shows the opposite relationship, with ca. 16–11 Ma calc-alkaline lavas comprising the lower half of the succession and ca. 11–10 Ma transitional lavas making up the most recent eruptive products (Skulski et al., 1992). The presence of calc-alkaline chemistries, as well as similar isotopic compositions to western WA rocks, suggest that a mid-Miocene period of volcanism in the St. Clare Creek volcanic field was influenced by subduction. However, the alkaline, intraplate-like nature of the lowermost Wolverine lavas (intermediate between Cordilleran intra-plate and arc magmas; e.g., Eiché et al., 1987; Skulski et al., 1991) suggests that subduction input was not

constant through the lifetime of the Wolverine volcanic center, and melting of a subduction-affected mantle wedge did not always occur in this location (Fig. 1). To explain the geochemistry of the Wolverine center, Skulski et al. (1992) suggested that extension across the right-lateral Duke River and Denali faults (i.e., transtension) and associated low-degree melting of asthenosphere were responsible for the alkaline lavas. Abundant north-trending dikes are consistent with transtension between the northwest-trending strike-slip faults (Skulski et al., 1992). A gradual upsection change to more subduction-related input created the transitional to calc-alkaline chemistries. The opposite trend seen in the Klutlan center reflects a decreased subduction input.

The SCVF is located adjacent to the United States–Canada border in Alaska, ~30 km southwest of the Denali fault and ~30 km east of the Totschunda fault, ~60 km northeast of Mount Churchill and the modern slab edge (Fig. 1). The SCVF contains the oldest known WA lavas, including a basalt that yielded a $^{40}\text{Ar}/^{39}\text{Ar}$ age of ca. 30 Ma (Brueseke et al., 2019), which has been interpreted to represent the onset of WA magmatism (Richter et al., 1990; Brueseke et al., 2019). The SCVF is ~18 km × ~28 km in size, and much of it was mapped by Richter et al. (2000), who also provided major-element chemical analyses of 18 SCVF rocks. Within the SCVF, several different eruptive packages that are geochemically and temporally distinct crop out, and we discuss these packages below. We adopt the geochemical framework of Preece and Hart (2004) and Trop et al. (2012) as a means of understanding the roles of intra-arc extension, subduction, and slab-edge effects in the petrogenesis of older phases of WA magmatism. Our field, geochemical, and geochronological results constrain the nature and timing of volcanism within the discrete SCVF, the oldest known part of the WA.

METHODS

Samples were collected to maximize stratigraphic relationships and to obtain a representative set of the mapped rock units of Richter et al. (2000). The geological units we display on Figure 2 are geographically constrained, time-transgressive petrologic units (based on observed physical, petrographic, and geochemical heterogeneities, following Brueseke and Hart [2008]) that encompass multiple units previously defined by Richter et al. (2000). Only the freshest samples were collected, and splits of most samples were made for both geochemistry and geochronology, from the same sample. A subset of splits of the same samples were processed for geochronology ($n = 60$) and geochemistry ($n = 60$).

Fourteen samples were previously analyzed through traditional $^{40}\text{Ar}/^{39}\text{Ar}$ step-heat geochronology at the University of Alaska Fairbanks Geochronology Lab and published in Brueseke et al. (2019). Forty-six different igneous rock samples were analyzed by $^{40}\text{Ar}/^{39}\text{Ar}$ geochronology at the University of Alaska Fairbanks Geochronology Lab using the single-grain fusion $^{40}\text{Ar}/^{39}\text{Ar}$ geochronology method (Broussard et al., 2018). Rock samples were crushed using a stainless-steel mortar and pestle, then sieved using 500–1000 micron

sieves. Samples were then washed and sonically bathed in deionized water to remove and decant clay particles. Samples were then dried in an oven overnight at $-60\text{ }^{\circ}\text{C}$, and homogeneous grains were hand-picked under an optical microscope to select phenocryst-free groundmass chips as well as hornblende and biotite mineral separates. The monitor mineral TCR-2 with an age of 28.619 Ma (Renne et al., 2010) was used to monitor neutron flux and calculate the irradiation parameter (J) for all samples. The samples and standards were wrapped in aluminum foil and loaded into aluminum cans of 2.5 cm diameter and 6 cm height. Mineral separates were sent to the uranium-enriched research reactor of McMaster University in Hamilton, Ontario, Canada, and irradiated for 20 megawatt-hours. After irradiation, samples were loaded into 2-mm-diameter holes in a copper tray and loaded in an ultra-high vacuum extraction line. The monitors were fused, and samples were heated, using a 6 W argon-ion laser following the technique described in York et al. (1981), Layer et al. (1987), and Benowitz et al. (2014). Argon purification was achieved using a liquid nitrogen cold trap and a SAES Zr-Al getter at $400\text{ }^{\circ}\text{C}$. The samples were analyzed in a VG-3600 mass spectrometer. The argon isotopes measured were corrected for system blank and mass discrimination, as well as calcium, potassium, and chlorine interference reactions following procedures outlined in McDougall and Harrison (1999). Typical full-system 8 min laser blank values (in moles) were generally $2 \times 10^{18}\text{ mol }^{40}\text{Ar}$, $3 \times 10^{18}\text{ mol }^{39}\text{Ar}$, $9 \times 10^{18}\text{ mol }^{38}\text{Ar}$, and $2 \times 10^{18}\text{ mol }^{36}\text{Ar}$, which are 10–50 times smaller than the sample/standard volume fractions. Correction factors for nucleogenic interferences during irradiation were determined from irradiated CaF_2 and K_2SO_4 as follows: $(^{39}\text{Ar}/^{37}\text{Ar})_{\text{Ca}} = 7.06 \times 10^4$, $(^{36}\text{Ar}/^{37}\text{Ar})_{\text{Ca}} = 2.79 \times 10^4$, and $(^{40}\text{Ar}/^{39}\text{Ar})_{\text{K}} = 0.0297$. Mass discrimination was monitored by running calibrated air shots. The mass discrimination during these experiments was 0.8% per mass unit. The majority of samples were analyzed using a single-grain or multi-grain fusion analysis approach. We developed a procedure to limit the effects of alteration by degassing each sample at 0.5 W for 60 seconds, and the released gas was pumped off for time efficiency and hence increased throughput. The results have a single-grain and/or multi-grain precision of 1%. A subset of 14 samples was selected for higher-precision ages and step-heated from relatively low temperatures until reaching fusion temperatures using the 6 W argon-ion laser (Benowitz et al., 2014). For each step, isotopic ratios of Ar were determined, with a range of mean square of weighted deviates (MSWD) values of 0.0–6.25 (Table S1¹).

A summary of 46 new $^{40}\text{Ar}/^{39}\text{Ar}$ single-grain fusion ages is given in Table S1 (footnote 1) with all ages quoted to the ± 1 sigma level and calculated using the constants of Renne et al. (2010). The integrated age is the age given by the total gas measured and is equivalent to a potassium-argon (K-Ar) age. The age spectrum provides a plateau age, if three or more consecutive gas fractions represent at least 50% of the total gas release and are within two standard deviations of each other (MSWD < 2.5). When possible, inverse isochron ages were calculated from an inverse isochron diagram of $^{36}\text{Ar}/^{40}\text{Ar}$ versus $^{39}\text{Ar}/^{40}\text{Ar}$ ratios measured during each heating step (Roddick, 1978; Roddick et al., 1980; Benowitz et al., 2011).

For geochemistry, fist-sized samples were split into smaller pieces using a hydraulic press with tungsten splitting jaws. All weathered surfaces were removed by cutting with a rock saw and grinding on a 60-grit grinding wheel. All samples were cleaned in deionized water with an ordinary toothbrush and allowed to dry completely. When dry, all samples were crushed to pea-size and smaller fragments using tungsten crushing plates of the RockLabs hydraulic press, then randomized using a coning and quartering method on a glass plate. A small amount ($\sim 25\text{ mL}$) of crushed sample was powdered using a Spex Industries shatterbox and an Alumina shatterbox assembly for eight minutes.

Fifty-five rock sample powders were sent to Washington State University for X-ray fluorescence (XRF) analysis of major elements, minor elements, and select trace elements (Si, Ti, Al, Fe, Mn, Mg, Ca, Na, K, P, V, Ni, Cr, Ga, Cu, and Zn) and inductively coupled plasma–mass spectrometry (ICP-MS) analysis of select trace- and rare-earth elements (Ba, Th, Nb, Y, Hf, Ta, U, Pb, Rb, Cs, Sr, Sc, Zr, La, Ce, Pr, Nd, Sm, Eu, Gd, Tb, Dy, Ho, Er, Tm, Yb, and Lu). Analyses occurred via a ThermoARL Advant'XP+ sequential X-ray fluorescence spectrometer and an Agilent 7700 ICP-MS following the methods of Johnson et al. (1999) and Gaschnig et al. (2011). Five samples (SB15-30, 15JB16LA, 15JB28LA, 15JB31LA, and 15JB41LA) were analyzed for major-element (Si, Al, Fe, Mn, Mg, Ca, Na, K, and P) and trace-element (Rb, Sr, Y, Zr, V, Ni, Cr, Nb, Ga, Cu, Zn, Co, Ba, La, Ce, U, Th, Sc, and Pb) chemistry via a Panalytical PW 4204 XRF spectrometer at Franklin and Marshall College, following the methods outlined in Mertzman (2000, 2015) and online at <http://www.fandm.edu/earth-environment/laboratory-facilities/>. Total volatiles loss-on-ignition (LOI) values were determined for each sample. Major elements are reported as wt% oxide, and trace-element concentrations are presented as parts per million (ppm). All major-, trace-, and rare-earth element data are presented in Table S2 (footnote 1). Fe was split according to LeMaitre (1976), and all major-element data used in diagrams and the discussion are reported as anhydrous using the split Fe data.

Although care was taken in the field to collect the freshest possible samples of volcanic rocks, LOI values and petrographic evidence suggest that some samples have been affected by secondary hydrothermal and/or meteoric fluid alteration and/or weathering. Based on a sample containing one or more of: (1) petrographic observations of abundant secondary phyllosilicate and/or carbonate phases; (2) LOI > 3.5 wt%; and/or (3) anomalous (i.e., non-igneous) relationships between Mg, Fe, Ni, Cr, V, and Sc, nine samples were interpreted to be altered and possess non-primary geochemical traits and were excluded from further consideration (reported in Table S2).

RESULTS

Field Relations and Geochronology

Field work in 2015 consisted of a week of targeted sampling and stratigraphic section measuring; time constraints did not permit targeted geologic mapping. Sample locations are summarized in Table S2 (footnote 1) and on

¹Supplemental Files. Complete spectra and laser-fusion $^{40}\text{Ar}/^{39}\text{Ar}$ data and whole-rock geochemistry. Please visit <https://doi.org/10.1130/GES02114.S1> or access the full-text article on www.gsapubs.org to view the Supplemental Files.

Figure 2. Detailed petrographic descriptions of all SCVF samples can be found in Berkelhammer (2017). A summary of step-heat geochronology is found in Table 1 and Figure 3; the complete spectra and laser-fusion ⁴⁰Ar/³⁹Ar data are presented in the Supplemental Files (Table S1). Photographs of outcrops and field relations are shown in Figure 4 and Figure S1. Representative photomicrographs from SCVF units are shown in Figure S2. Rock units from the SCVF are named based on geographic location and chemical composition and are divided into six units: (1) Rocker Creek volcanics; (2) Ptarmigan Creek volcanics, which include two suites of silicic materials; (3) Cabin Creek volcanics and Sonya Creek shield volcano; (4) Flat Top volcanics; (5) Young Creek volcanics; and (6) Border lavas; Fig. 2). Refer to Supplemental Files (footnote 1) for sample locations and Figure 2 for how our units compare to SCVF map units defined by Richter et al. (2000).

Rocker Creek Volcanics

Rocker Creek volcanics are primarily poorly exposed, blocky lavas that crop out mainly in small gullies along Rocker Creek (Fig. 4; Fig. S1). Rocker Creek lavas are intruded by domes and subvolcanic rocks (Richter et al., 2000). Petrographically, Rocker Creek lavas are clinopyroxene-plagioclase-phyric with a glassy or microcrystalline groundmass consisting of plagioclase laths, opaque oxide minerals, and/or clinopyroxene. Only a basaltic sample contains

olivine. More evolved rocks have hornblende and biotite phenocrysts. Rocker Creek lavas yield 30.9 (±0.85)–23.4 Ma ⁴⁰Ar/³⁹Ar ages (Table 1). The Rocker Creek volcanics also include lava domes that occur as platy and blocky outcrops of hornblende plagioclase-phyric rock (Fig. 4). They have a glassy, microcrystalline groundmass consisting of aligned and/or flow-banded plagioclase laths and opaque minerals. Rocker Creek domes yield 26.0–23.2 Ma ⁴⁰Ar/³⁹Ar ages (Table 1). Other Rocker Creek volcanic rocks are exposed north of Ptarmigan Lake (Fig. 2). These yield >28 Ma ages and were originally mapped by Richter et al. (2000) as unit Tdh (our Ptarmigan Creek volcanics) (Fig. 2; Table 1).

Ptarmigan Creek Volcanics

The Ptarmigan Creek volcanics are located physically between the Rocker Creek volcanics and the Sonya Creek shield volcano (Cabin Creek volcanics), and they are dominated by two primary chemical suites: (1) a package that ranges chemically from basaltic andesite to dacite (Ptarmigan Creek intermediate rocks) and (2) a second suite of more silicic rocks (Ptarmigan Creek silicic rocks) with SiO₂ >72 wt%; this suite also includes samples that meet geochemical criteria to be considered adakitic (see below). The Ptarmigan Creek intermediate suite includes 23.2–21.7 Ma lavas, domes, plugs, and diorites (Fig. 4). These rocks show petrographic diversity. Two samples have cumulate textures of anhedral plagioclase crystals with intergranular biotite,

TABLE 1. SUMMARY OF NEW ⁴⁰Ar/³⁹Ar AGE RESULTS

Age (Ma)	Error	Sample no.	Unit	Age (Ma)	Error	Sample no.	Unit	Age (Ma)	Error	Sample no.	Unit
24.1	0.2	15LA	RC	22.1	0.3	43LA	No chemistry	23.9	0.2	SB-34	PC
24.8	0.3	16LA	RC	23.4	0.7	45LA	BL	23.7	0.6	SB-36	PC
25.9	0.4	17LA	RC	21.3	0.5	46LA	BL	28.0	3.1	SB-37	PC
22.6	0.7	20LA	RC	27.0	0.4	47LA	BL	24.6	0.3	SB-39	FT
27.5	0.4	20LATUFF	No chemistry	21.4	0.1	49LA	RC	19.3	0.1	SB-40	FT
26.2	1.2	26LA	RC	30.3	3.1	MINIVOLCANO	RC	19.7	0.1	SB-41	FT
22.9	0.2	27LA	RC	21.3	0.1	SB-17	CC	23.0	0.2	SB-43	PC
23.2	0.2	28LA	RC	19.7	0.4	SB-18	CC	25.6	0.2	SB-44	No chemistry
24.5	0.6	30LA	RC	23.3	0.3	SB-19	CC	20.3	0.1	SB-45	PC
23.4	0.5	31LA	RC	22.1	0.4	SB-20	CC	22.6	0.2	SB-46	PC
22.3	0.3	32LA	No chemistry	22.5	0.2	SB-23	CC	22.2	0.1	SB-47	PC
26.0	0.2	33LA	RC	22.1	0.2	SB-24	CC	21.7	0.3	SB-48	PC
26.6	0.5	34LA	RC	21.5	0.4	SB-25	CC	25.3	1.2	SB-50	YC
27.5	0.5	35LA	No chemistry	20.7	0.4	SB-27	CC	20.2	0.7	SB-51	YC
19.6	0.5	37LA	RC	18.5	0.5	SB-28	CC	19.7	0.2	SB-52	YC
23.3	0.1	38LA	RC	21.3	0.5	SB-29	CC	21.3	0.5	SB-53	YC
23.2	0.2	39LA	RC	21.7	0.4	SB-30	CC	19.2	0.3	SB-54	YC
26.0	0.4	40LA	RC	21.7	0.6	SB-31	CC	19.1	0.2	SB-55	YC
23.5	0.2	41LA	RC	22.0	0.3	SB-32	CC	22.9	2.3	SB-56	YC
27.2	0.4	42LA	RC	29.0	0.2	SB-33	PC				

Note: Plateau ages in italics. BL—Border lavas; CC—Cabin Creek; FT—Flat Top; PC—Ptarmigan Creek; RC—Rocker Creek; YC—Young Creek.

clinopyroxene, amphibole, and quartz (in the dacite). The basaltic-andesite and andesite samples have extrusive textures, with plagioclase phenocrysts and altered mafic phases in a glassy groundmass. Two dacites have hornblende phenocrysts and are otherwise plagioclase-phyric lavas. The Ptarmigan Creek silicic suite includes lava domes that yield 24.8–23.3 Ma $^{40}\text{Ar}/^{39}\text{Ar}$ ages and a 20.3 ± 0.12 Ma plug (Table 1). These silicic rocks crop out as >300-m-tall domes, lavas in valleys, and as plugs (Fig. 4). They are porphyritic with plagioclase and sanidine phenocrysts in a microcrystalline to cryptocrystalline groundmass. Three samples have biotite phenocrysts, and one has hornblende and biotite phenocrysts. The adakitic samples are sanidine-phyric lavas with a microcrystalline and glassy groundmass.

Sonya Creek Shield Volcano: Cabin Creek and Flat Top Volcanics

Cabin Creek volcanics are from two stratigraphic sections on the north and south flanks of the Cabin Creek drainage in the Sonya Creek shield volcano. Cabin Creek lavas are flat lying to gently dipping and range in thickness from 10 to 50 m thick (Fig. 4). Most lavas have vesicular and oxidized basal and upper breccia zones that form slopes, while the massive lava interiors are cliff forming. Thin (50 cm), interbedded tuffaceous breccia occurs on the north side of Cabin Creek. Along the south side of Cabin Creek are dacite lavas with well-developed, ~30-m-tall columnar joints, as well as a package of four mafic lavas with interbedded volcanic breccias (Fig. 4). The south side has sedimentary units interbedded with lavas; a poorly sorted boulder conglomerate with rounded volcanic clasts is interpreted as a debris and/or hyperconcentrated-flow deposit, and a poorly sorted breccia with volcanic boulders up to one meter in size is interpreted as a lahar deposit (Fig. 4). These sedimentary units are likely inter-eruptional deposits on the flanks of the volcano. Lavas along the north side of Cabin Creek are two-pyroxene, plagioclase-phyric glomeroporphyritic lavas. Clinopyroxene phenocrysts are pink in plane-polarized light and are likely titanite. Plagioclase phenocrysts show varying degrees of disequilibrium textures, but sieve texture and embayments are common. The trachydacites and the trachyandesite from the top of the section on the south side of Cabin Creek are plagioclase-phyric and contain clinopyroxene phenocrysts. The lowermost rocks from the south side (“mafic package” of basaltic-andesites to andesites) are two-pyroxene, plagioclase-olivine-phyric glomeroporphyritic lavas. Clinopyroxene crystals may be titanite, and plagioclase phenocrysts show sieve texture. Cabin Creek volcanics yield 23.3–18.5 Ma $^{40}\text{Ar}/^{39}\text{Ar}$ ages (Table 1).

The Flat Top volcanics were collected in stratigraphic context from the southeast margin of the inferred Sonya Creek shield volcano. Flat Top volcanics include lavas, tuff, and interbedded lahar deposits (Fig. 4). Silicic lavas in this package are ~10-m-thick blocky outcrops with sparse interbedded air-fall tuff deposits (Fig. 4). The massively bedded rhyolite ash-flow tuff (Flat Top tuff) that caps the stratigraphy is ~30 m thick and has flattened pumice fragments and volcanic lithic fragments greater than 15 cm long (Fig. 4). The Flat Top tuff

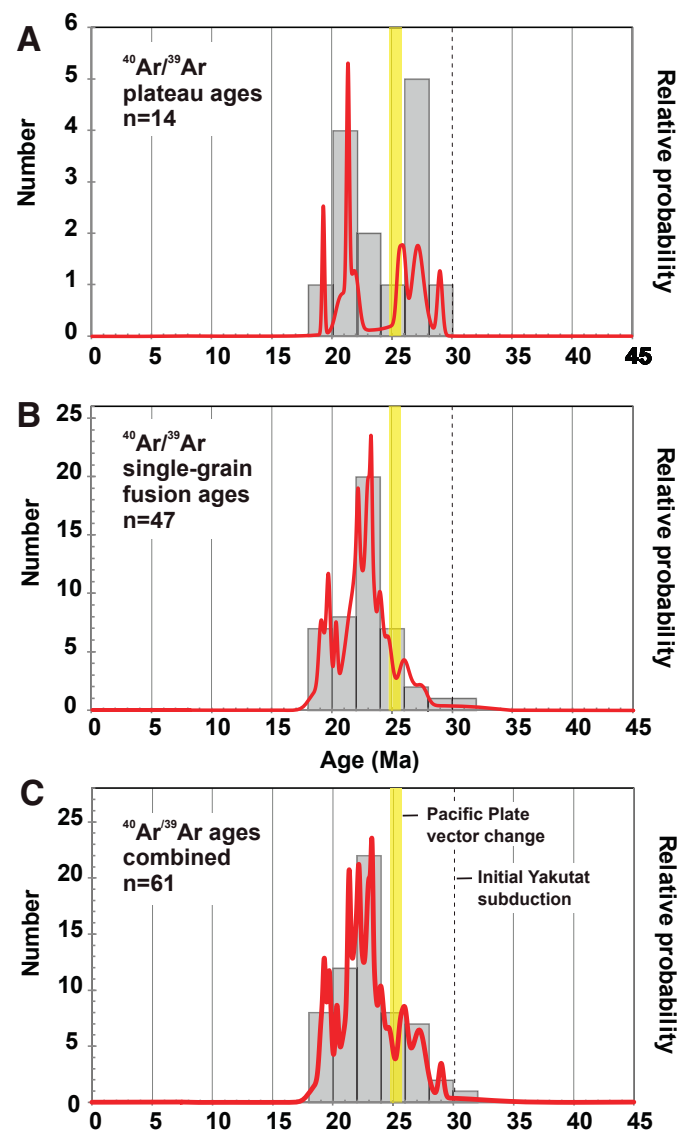


Figure 3. Histograms (gray bars) and age probability diagrams (red curves) for $^{40}\text{Ar}/^{39}\text{Ar}$ ages from volcanic bedrock samples from the Sonya Creek volcanic field. (A) Plateau ages (n = 14). (B) Single-grain fusion ages (n = 46). (C) Combined plateau and single-grain fusion ages (n = 60). Yellow vertical bar denotes change in Pacific plate vector (Jicha et al., 2018). Each curve is the sum of ages and uncertainties from all analyses of a set of samples. The area under each curve is normalized according to the number of constituent analyses. No volume constraints on magmatic activity through time (or per unit) are implied by these diagrams.

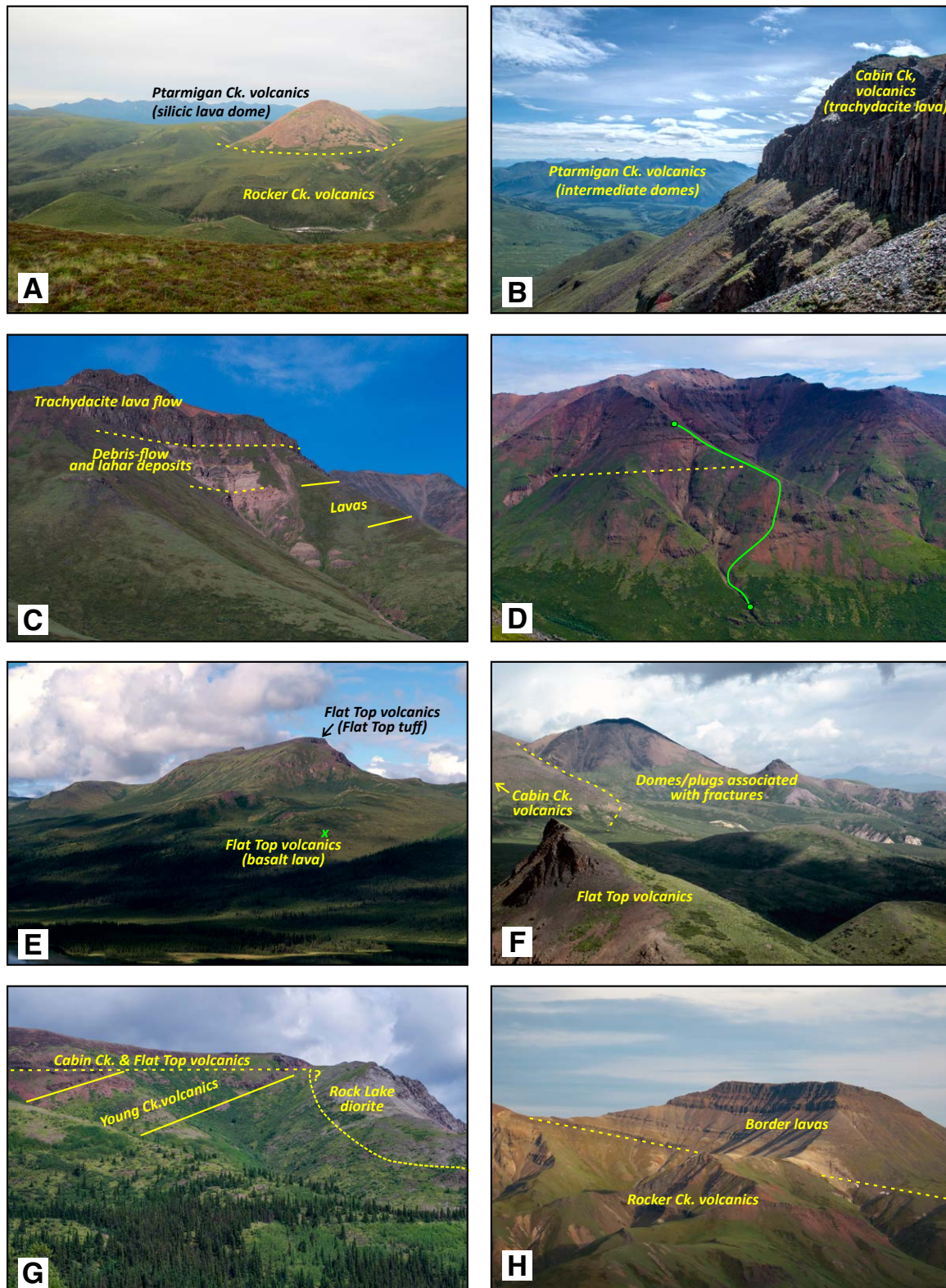


Figure 4. (A) The large Ptarmigan Creek silicic dome is ~300 m thick and was emplaced through the older Rocker Creek lavas. View to the east. (B) A view of the Ptarmigan Creek intermediate domes and hypabyssal diorite intrusives, with Cabin Creek volcanics in the foreground. (C) Photograph showing the south side of Cabin Creek section (see Fig. 2), with the lower mafic package, interbedded sedimentary strata, and thick upper trachydacite flow. (D) Cabin Creek volcanic package along north side of Cabin Creek and our sampling traverse (green line; Fig. 2). The dashed yellow line marks the approximate level below which the lavas dip more steeply to the west and above which have shallower dips. (E) View from distal Cabin Creek volcanics Flat Top hill. The location of the 24.6 Ma Flat Top basalt (SB15-39) is shown by the green X; the 19.3 Ma Flat Top tuff (SB15-40) is marked by the yellow arrow (e.g., capping unit). (F) View to the north from Flat Top hill, showing the large domes and plugs associated with marginal fractures of the Sonya Creek shield volcano. (G) Complex structural relationships of the northwest-dipping Young Creek volcanics, Rock Lake diorite (SB15-56), and flat-lying rocks of the Sonya Creek shield volcano (e.g., Cabin Creek volcanics) and Flat Top volcanics. View to the northeast. (H) View of an ~400-m-thick section of the Border lavas in the upper Rocker Creek showing them overlying the Rocker Creek volcanics. These lavas are across the border in Yukon Territory, Canada. View to the southeast.

is found only along the southeast margin of the Sonya Creek shield volcano (as mapped by Richter et al., 2000). Rocks from the Flat Top volcanics show some petrographic diversity. The basalt from the bottom of the section is a clinopyroxene-plagioclase-olivine-phyric lava in coarse-grained groundmass. The Flat Top tuff (SB15-40) has embayed plagioclase, anorthoclase, and sanidine phenocrysts, and rare clinopyroxene. The groundmass is cryptocrystalline with a vitrophyric to eutaxitic texture, showing welded pumice fragments (Fig. 4). The two trachydacites are crystal-poor lavas. The Flat Top volcanics are ca. 25–19 Ma, judging from a basalt at the base of the sampled stratigraphy that yields a $^{40}\text{Ar}/^{39}\text{Ar}$ age of 24.6 Ma and two lavas higher in the section that yield $^{40}\text{Ar}/^{39}\text{Ar}$ ages of 19.7 Ma and 19.3 Ma (Table 1).

Young Creek Volcanics and Border Lavas

Young Creek volcanics crop out as massive clinopyroxene-plagioclase phyric lavas that dip to the northwest and are intruded by a north-striking dike (Figs. 2 and 4G). Two basaltic andesites contain olivine, and one of the andesites is hornblende bearing. A diorite intrusive body is exposed along Rock Lake (Figs. 2 and 4G) and has a cumulate texture of large plagioclase crystals with intergranular clinopyroxene and biotite; the diorite is included

with Young Creek volcanics on geochemical plots presented below because of similar geochemistry, age, and geographic extent (Richter et al., 2000; Berkelhammer, 2017). Young Creek rocks yield 21.3–19.1 Ma $^{40}\text{Ar}/^{39}\text{Ar}$ ages; the Rock Lake diorite is 22.9 Ma with a large error (± 2.2 Ma) (Table 1).

The Border lavas (Fig. 2) depositionally overlie the Rocker Creek volcanics (Fig. 4H) but are age-correlative with Young Creek volcanics and are included with those on chemical plots (see geochemistry section below). This package includes volcanoclastic rocks (Richter et al., 2000). Sampled Border lavas are plagioclase-phyric with a glassy and microcrystalline groundmass, including embayed plagioclase crystals that show sieve texture and opaque pseudomorphs after hornblende (Fig. 5). The Border lavas yield 21.3 and 19.6 Ma $^{40}\text{Ar}/^{39}\text{Ar}$ ages (Table 1).

Geochemical Classification and Bulk-Rock Geochemistry

A total alkali versus silica (TAS) diagram after LeBas et al. (1986) shows the SCVF rocks spanning a compositional range from sub-alkaline basalt through rhyolite, with some samples plotting within the transitional fields of trachyandesite and trachydacite (Fig. 5). Most SCVF rocks plot as medium-K on the classification diagram of Gill (1981), but ten samples from Cabin Creek,

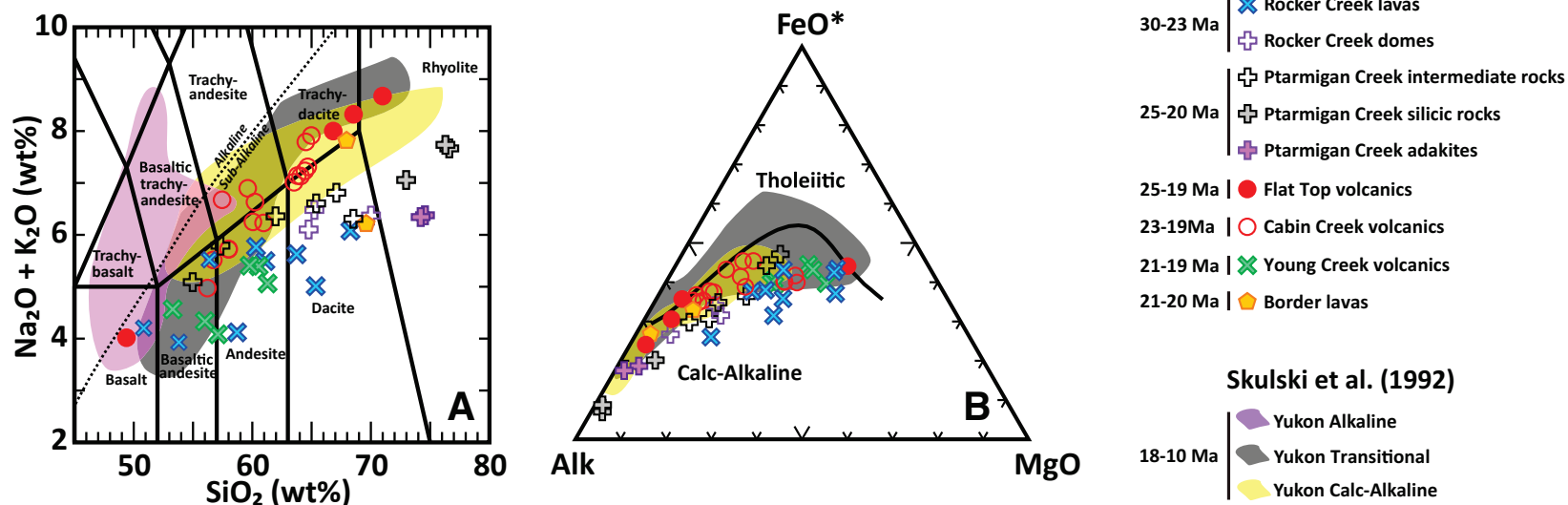


Figure 5. (A) Total alkali silica diagram after Le Bas et al. (1986), with the alkaline/sub-alkaline discrimination line of Irvine and Baragar (1971). (B) AFM discrimination diagram after Irvine and Baragar (1971). Data for Yukon alkaline, transitional, and calc-alkaline fields are ca. 18–10 Ma eastern Wrangell Arc samples from Skulski et al. (1991, 1992). All other figures that depict chemical data use the symbols and fields depicted in this figure legend.

Flat Top, and Ptarmigan Creek show a high-K array (Fig. 6). An AFM diagram after Irvine and Baragar (1971) shows that all SCVF intermediate samples are calc-alkaline, with some of the Cabin Creek and Flat Top rocks plotting along the divide between the calc-alkaline and tholeiitic fields (Fig. 6). A FeO^*/MgO versus wt% SiO_2 diagram after Miyashiro (1974) shows most of the Flat Top and Cabin Creek rocks (as well as one Border lava and one Ptarmigan Creek adakitic lava) plotting within the tholeiitic field, while the remainder of the SCVF rocks plot as calc-alkaline (Fig. 6). Because the Flat Top and Cabin Creek rocks are sub-alkaline to transitional on a TAS diagram, and they plot as either calc-alkaline or tholeiitic depending on what classification diagram is used, they will be referred to as “transitional tholeiitic” in geochemical discussions. This term was used by Preece and Hart (2004) to describe their trend 1 magma series, and because Flat Top and Cabin Creek rocks are geochemically similar to trend 1 rocks, we adopt a similar approach. No SCVF rocks show similar chemistry to the primitive alkaline and transitional volcanic rocks from WVB volcanic fields in Canada (Figs. 5 and 6; Skulski et al., 1991, 1992), and these fields are not included on additional plots of geochemistry.

All SCVF samples with $\text{SiO}_2 > 65$ wt% are plotted on discrimination diagrams for silicic rocks (Fig. 7). SCVF rocks plot as peraluminous to metaluminous based on the alumina saturation index (Frost and Frost, 2008; Fig. 7). The Y versus Nb discrimination diagram after Pearce et al. (1984) shows that three Flat Top rocks plot in the within-plate granite field, while the remainder of the SCVF silicic rocks plot in the volcanic arc field (Fig. 7). Similarly, the same Flat Top rocks plot in the “A-type granite” field, and the remainder plot in the “I & S-types granite” field on the discrimination diagram of Whalen et al. (1987) (Fig. 7). This indicates that the geochemistry of the three silicic Flat Top rocks

(two lavas and the 19.3 Ma Flat Top tuff) reflects processes that formed “hot and dry felsic” magmas, which is consistent with their anhydrous mineralogy.

Major-element concentrations for SCVF rocks are plotted on Harker diagrams to show geochemical arrays with differentiation (Figs. 8 and 9). All SCVF rocks show decreasing wt% TiO_2 , Al_2O_3 , FeO^* , MnO , MgO , P_2O_5 , and CaO values with increasing SiO_2 , but Flat Top and Cabin Creek rocks tend to have higher amounts of TiO_2 and P_2O_5 and lower amounts of MgO and CaO for a given SiO_2 content (Fig. 8). Conversely, Rocker Creek and Young Creek rocks tend to have lower TiO_2 and P_2O_5 and higher MgO and CaO at a given SiO_2 value. All SCVF rocks show increasing K_2O and Na_2O values with increasing SiO_2 (Fig. 8). Flat Top and Cabin Creek rocks tend to have higher values of both, while Rocker Creek and Young Creek rocks tend to have lower values, at a given SiO_2 content. The Ptarmigan Creek intermediate rocks have major-element compositions that are intermediate between the Flat Top and Cabin Creek rocks and Rocker Creek suite (i.e., TiO_2 , MgO , and K_2O). The Ptarmigan Creek silicic rocks (72.9–76.5 wt% SiO_2) show arrays that are different from the intermediate rocks. The silicic rocks show a sharp decrease in Al_2O_3 content at high SiO_2 values and lower Na_2O values (3.7–4.6 wt%) than Flat Top silicic volcanics (4.9–5.3 wt%). Three of the Ptarmigan Creek silicic rocks belong to the high-K array, and the two Ptarmigan Creek adakites belong to the medium-K array (Fig. 8). Flat Top and Cabin Creek rocks plot within the field for trend 1 data of Preece and Hart (2004) and the “calc-alkaline” field of WA rocks in Canada (Skulski et al., 1991, 1992), discussed later.

Trace-element values for SCVF rocks are plotted on Harker diagrams to show geochemical arrays (Fig. 9). All SCVF rocks show decreasing values of the compatible trace elements (Sr, Ni, Sc, Cr, Cu, Zn, and V) with increasing

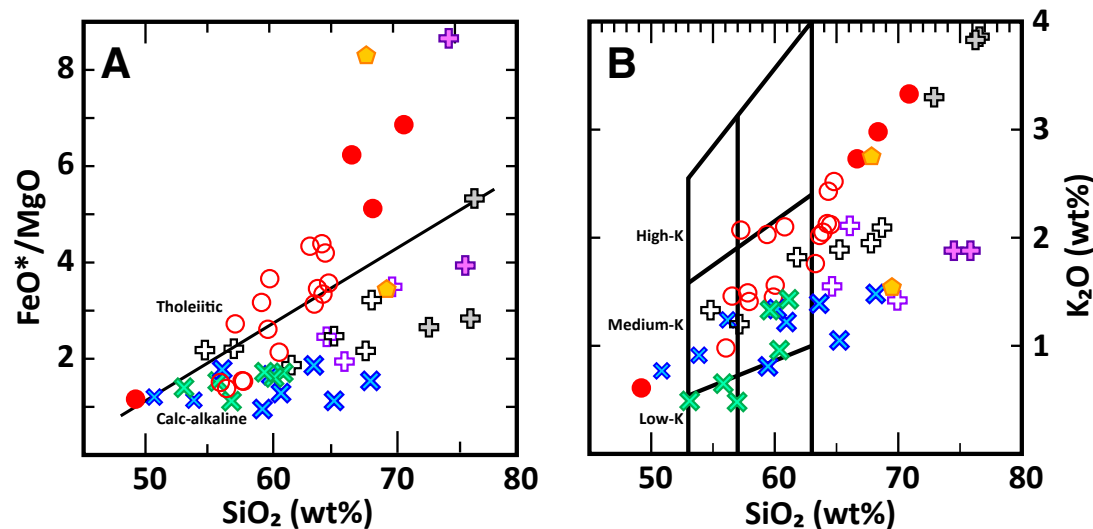


Figure 6. (A) FeO^*/MgO versus SiO_2 wt% discrimination diagram after Miyashiro (1974). (B) Gill (1981) andesite classification diagram based on K_2O . Symbols defined in Figure 5.

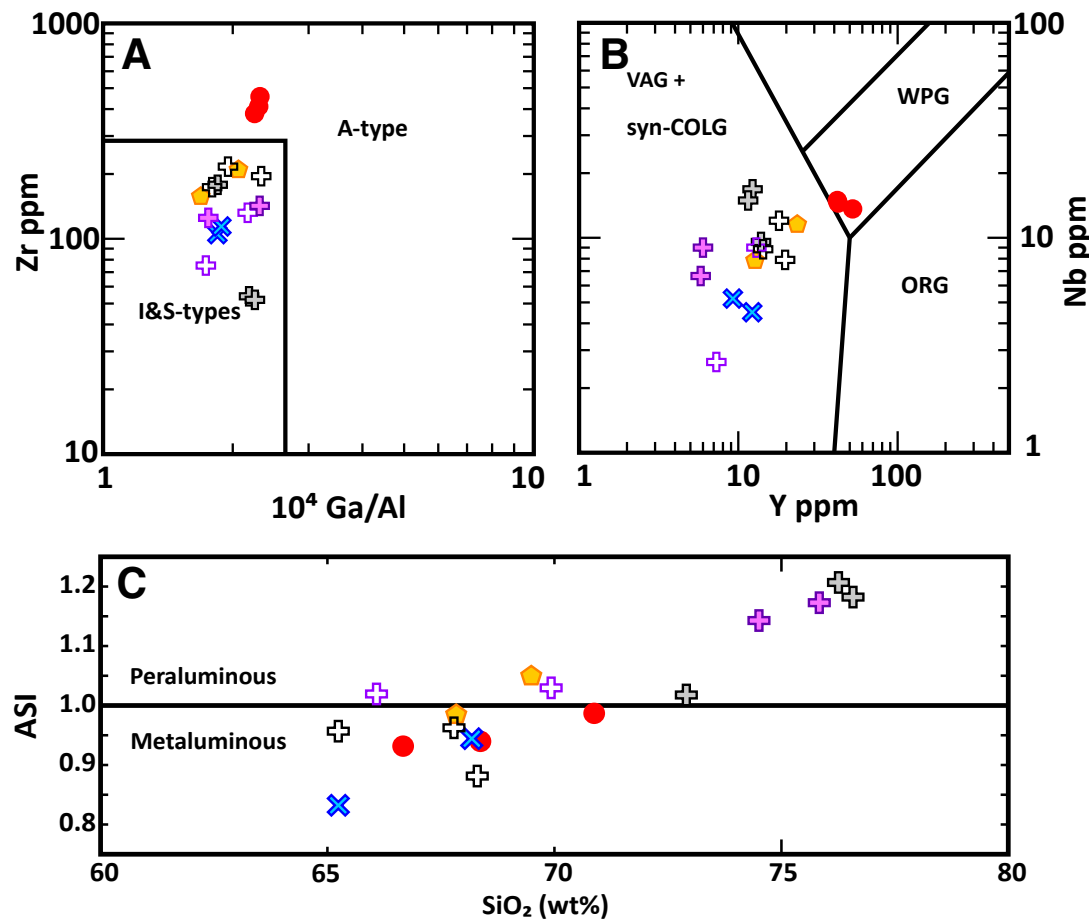


Figure 7. Felsic classification diagrams after (A) Whalen et al. (1987), (B) Pearce et al. (1984), and (C) Frost and Frost (2008). Symbols defined in Figure 5. COLG—collision granites; ORG—ocean ridge granites; VAG—volcanic arc granites; WPG—within-plate granites. I—igneous; S—sedimentary; A—anorogenic.

wt% SiO_2 content, but Flat Top and Cabin Creek rocks tend to have lower amounts of Sr, Ni, and Cr and higher Zn for a given SiO_2 content (Fig. 9; Table S2 [footnote 1]). Most Rocker Creek volcanics overlap with trend 2b calc-alkaline lavas of Preece and Hart (2004), the significance of which will be discussed later. All SCVF rocks show increasing values of the large ion lithophile elements (LILEs; Rb, Ba, U, Th, Pb, and Cs) with increasing SiO_2 , but Flat Top and Cabin Creek rocks tend to have higher concentrations of Rb, U, Th, Pb, and Cs at a given SiO_2 content (Fig. 9; Table S2). The Ptarmigan Creek silicic rocks show a wide range of these incompatible trace elements over a relatively restricted SiO_2 range. High field strength elements (HFSEs; Y, Zr, Nb, Hf, and Ta) show mixed arrays for SCVF rocks. Flat Top and Cabin Creek rocks show a strong increase in HFSE values with SiO_2 , especially for

Y, Zr, and Hf (Fig. 9; Table S2) and overlap with trend 1 transitional-tholeiitic rocks of Preece and Hart (2004) and “calc-alkaline” field of eastern WA rocks in Canada (Skulski et al., 1991, 1992). The intermediate domes have slightly higher Y values at a given SiO_2 value than the Rocker Creek rocks and overlap with trend 2a adakites of Preece and Hart (2004).

Selected rare-earth element (REE) values for SCVF rocks are plotted against SiO_2 in Figure 9. REE concentrations versus SiO_2 show a geochemical relationship that is similar to the HFSE, with Flat Top and Cabin Creek rocks showing an increase in REE concentrations with increasing SiO_2 and plotting within the “calc-alkaline” field for WA rocks in Canada (Skulski et al., 1991, 1992). Rocker Creek, Young Creek, and the Ptarmigan Creek intermediate rocks show no correlation or a broadly negative correlation of REE with increasing SiO_2

(Fig. 9). In fact, the negative correlation for Rocker Creek, Young Creek, and the Ptarmigan Creek intermediate rocks is more evident with increasing atomic number; the light rare-earth elements (LREEs), especially La and Ce, show no obvious relationship, but the middle and heavy rare-earth elements (MREEs and HREEs) show a more defined negative variation with SiO_2 (Fig. 9; Table S2 [footnote 1]). Rocker Creek volcanics have similar REE profiles, with absent or small positive Eu-anomalies (Fig. 10). The one basalt (15JB25LA) is highlighted to show its generally higher trace-element abundances. The Ptarmigan Creek intermediate rocks show similar chondrite-normalized REE patterns, with subdued negative or positive Eu anomalies (Fig. 10). The Ptarmigan Creek silicic rocks have lower normalized values and more significant negative Eu anomalies (Fig. 10). An exception is the Ptarmigan Creek adakitic lava (15JB15LA), which has a steeper REE profile (i.e., higher LREE/HREE ratio) and a slight positive Eu anomaly. Flat Top rocks show variety in their REE profiles. Flat Top silicic rocks have more elevated chondrite-normalized REE values and show negative Eu/Eu* anomalies (Fig. 10), while the basalt from lower in the stratigraphic section (SB15-39) shows a very different REE profile, with lower REE values and a slight positive Eu/Eu* anomaly (Fig. 10). Cabin Creek rocks are similar to the Flat Top REE profiles but with slightly lower values and with more subdued negative Eu/Eu* anomalies (Fig. 10). Young Creek rocks and Border lavas show REE profiles that are similar to Rocker Creek lavas and domes, but the Border lavas have slightly steeper REE profiles (Fig. 10).

Multi-element diagrams of SCVF rocks, normalized to the primitive mantle values of Sun and McDonough (1989), show important geochemical differences and similarities (Fig. 11). Notably, all SCVF rocks show the enrichment in LILE and depletion in HFSE that are characteristic of subduction-related magmatism. The Rocker Creek volcanics show similar profiles to the Ptarmigan Creek intermediate rocks but with lower normalized trace-element values, particularly for REE (Fig. 11). The Ptarmigan Creek silicic rocks have higher values for the most incompatible trace elements but have similar REE values to Rocker Creek volcanics and Ptarmigan Creek intermediate rocks (Fig. 11). The Flat Top silicic rocks have very similar normalized trace-element values with HFSE depletion and LILE enrichment (Fig. 11). The basalt from lower in the Flat Top stratigraphic section shows a very different trace-element profile, with much lower normalized trace-element values and a lack of large Sr, P, or Ti anomalies, as well as much less pronounced HFSE depletion and LILE enrichment (Fig. 11). The lavas of Cabin Creek are very similar to each other, except for the basaltic andesite that is the most primitive rock from the Cabin Creek section (Fig. 11). Most of the Young Creek volcanics are similar to Rocker Creek and Cabin Creek rocks (Fig. 11). However, the Rock Lake diorite (SB15-56) has a distinctly different profile, with larger depletions in HFSE and REE and higher Sr values. The two Border lavas are plotted with the Young Creek volcanics, based in part on geochronological data, and have a similar geochemical profile (Fig. 11).

Select trace-element ratios are plotted against SiO_2 in Figure 12 to show geochemical characteristics that are helpful in classifying some of the rock types. Sr/Y ratio versus SiO_2 shows most of the Rocker Creek volcanics have higher Sr/Y values at a given SiO_2 content than the other rock groups,

particularly Flat Top and Cabin Creek rocks (Fig. 12A). At lower SiO_2 values, the Young Creek volcanics are also elevated in Sr/Y relative to the Cabin Creek rocks. This high Sr/Y array serves to further distinguish the Rocker Creek volcanics from the Ptarmigan Creek intermediate rocks. Ba/Nb, a ratio of fluid-mobile incompatible element to high field strength element, can also be used as a proxy for subduction input (Pearce et al., 2005). Ba/Nb ratios of SCVF rocks show a similar distinction between the Rocker Creek and Young Creek volcanics, in comparison to Flat Top, Cabin Creek, and Ptarmigan Lake volcanics (e.g., higher Ba/Nb at a given wt% SiO_2 ; Fig. 12B). Eu/Eu* quantifies the Eu anomalies shown on chondrite-normalized REE plots (Fig. 12C). When plotted against SiO_2 , the Ptarmigan Creek silicic rocks, the Flat Top silicic rocks, and the Cabin Creek volcanics show Eu/Eu* < 1 (0.9–0.37), values that are generally lower than Rocker Creek and Young Creek volcanics at a given SiO_2 content. The three most mafic samples from SCVF show the highest Eu/Eu* values (1.08–1.25; Fig. 12C). The Cabin Creek and Flat Top volcanics generally plot within the fields for “trend 1” data of Preece and Hart (2004), and the “calc-alkaline” field for Yukon WA rocks (Skulski et al., 1991, 1992). In summary, the bulk-rock geochemistry of SCVF rocks shows that a diverse suite of magmas erupted in the SCVF, all of which were affected by subduction zone processes in light of the variable major- and trace-element chemistries the rocks exhibit.

■ FIRST-ORDER CONSTRAINTS ON PETROGENESIS OF SCVF UNITS AND IMPLICATIONS

Rocker Creek Volcanics (30–23 Ma)

Rocker Creek lavas and domes show enrichment in LILE and HFSE depletion (relative to primitive mantle; Fig. 11), as well as elevated Sr/Y values (Fig. 12A), all of which suggests the role of fluids fluxing from the subducting oceanic plate and subsequent melting of mantle-wedge peridotite (Stern, 2002). Rocker Creek lavas and domes have elevated Ba/Nb values (Figs. 11 and 12B), suggesting that they formed under oxidizing conditions in the presence of H_2O and other volatile phases liberated from the subducting slab. The Rocker Creek lavas and domes also contain hornblende and biotite phenocrysts consistent with a role of H_2O in their source and a subduction origin.

Eu/Eu* provides an indication of the oxidation state of a magma, where values less than 1 indicate a reducing environment (i.e., a greater proportion of Eu^{2+} to Eu^{3+}) and a role for plagioclase as a fractionating phase (i.e., distribution coefficient for Eu in plagioclase increases as proportion of Eu^{2+} increases; Drake, 1975; Drake and Weill, 1975). Rocker Creek lavas and domes have Eu/Eu* values close to 1 (Fig. 12C), suggesting that Eu was dominantly in the Eu^{3+} valence state, also indicating that the magma was oxidized. Rocker Creek domes are slightly younger and generally more evolved than Rocker Creek lavas (Table 1 and Figs. 8 and 9) and may represent the late-stage silicic phases of the same vent source that were too viscous to flow as far as the older lavas. Consequently, the eruptive source for Rocker Creek lavas and domes

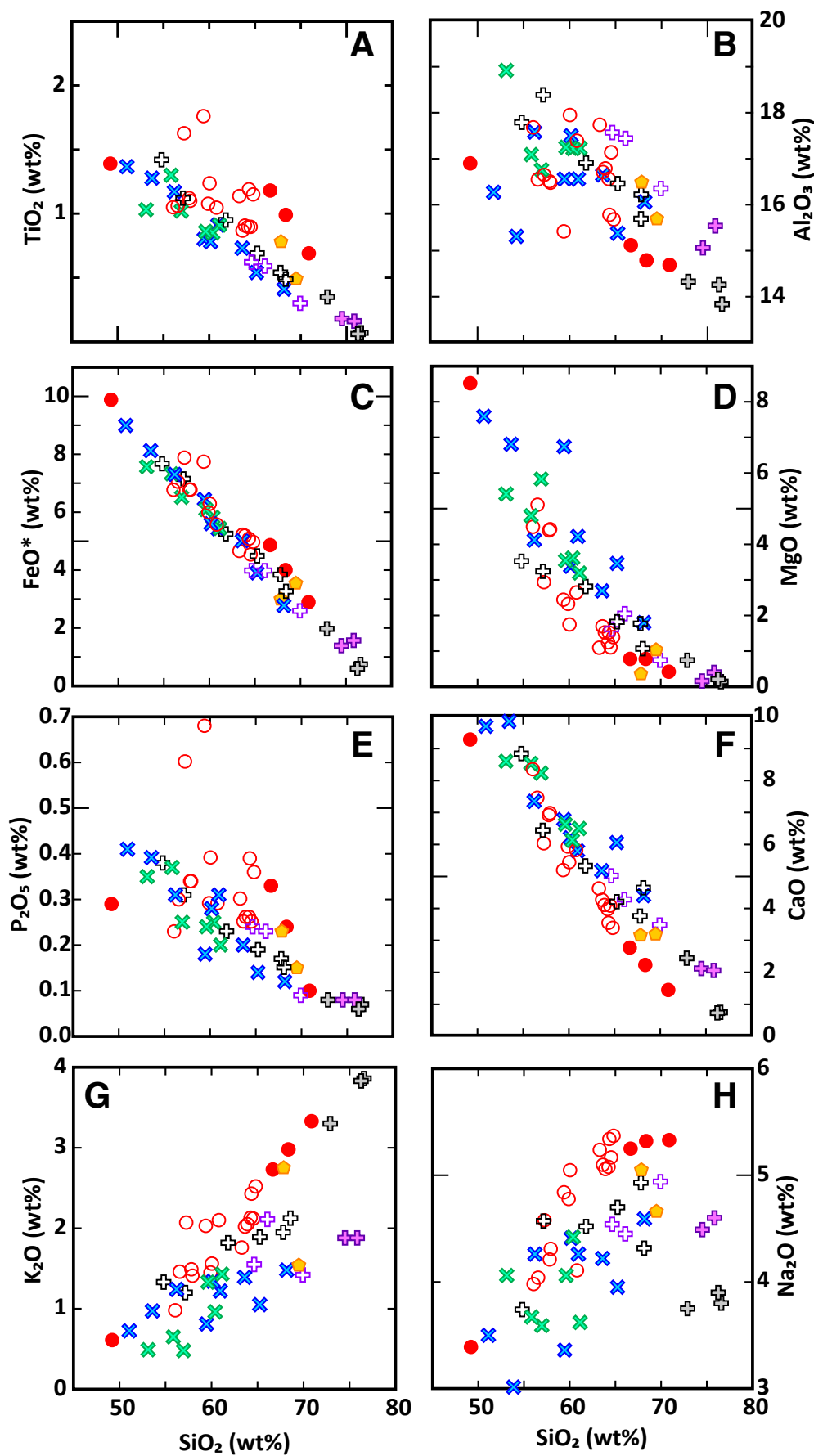


Figure 8. Harker diagrams illustrating major-element variations with wt% SiO₂. Symbols defined in Figure 5.

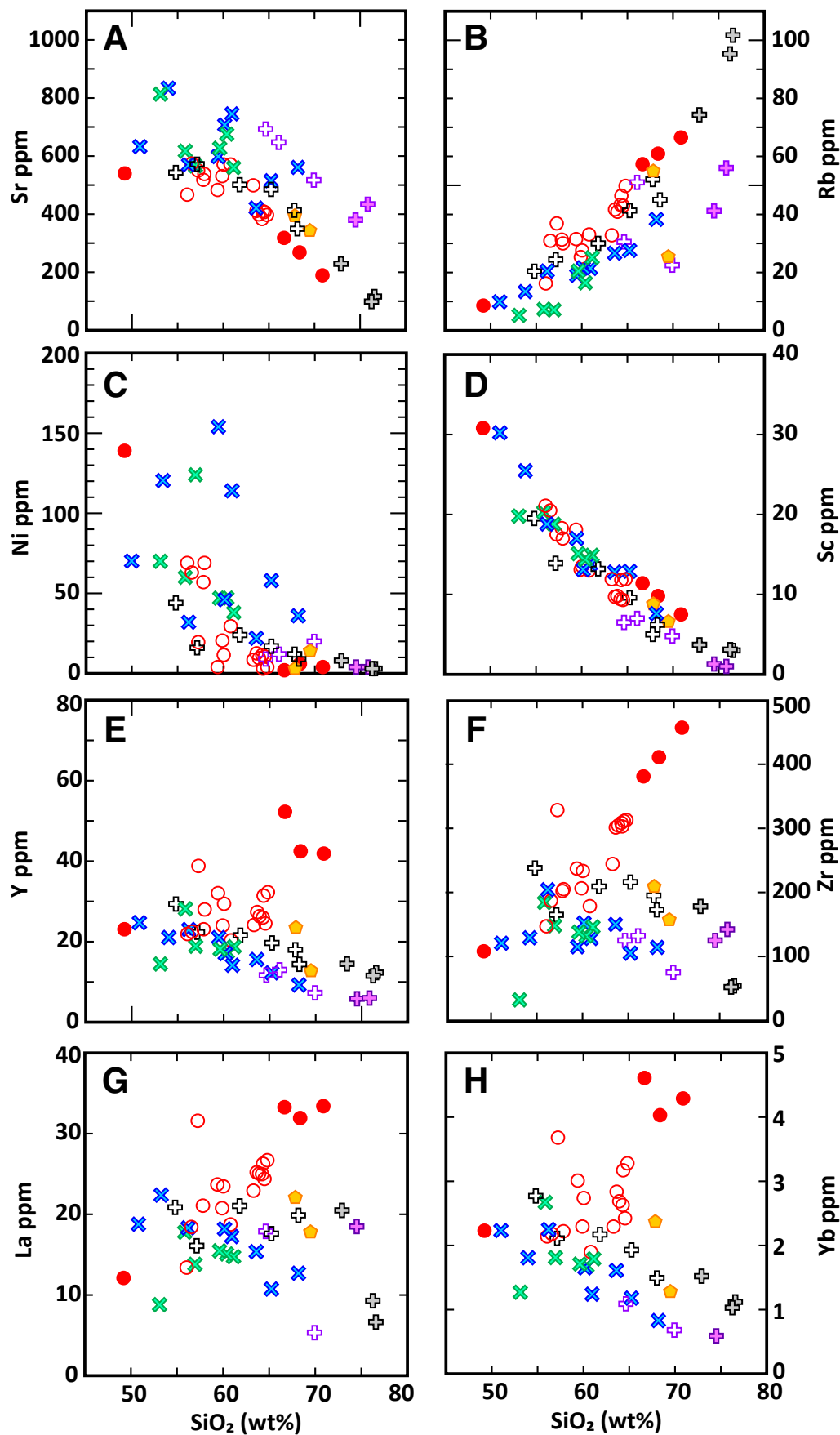


Figure 9. Harker diagrams illustrating selected trace-element variations with wt% SiO₂. Symbols defined in Figure 5.

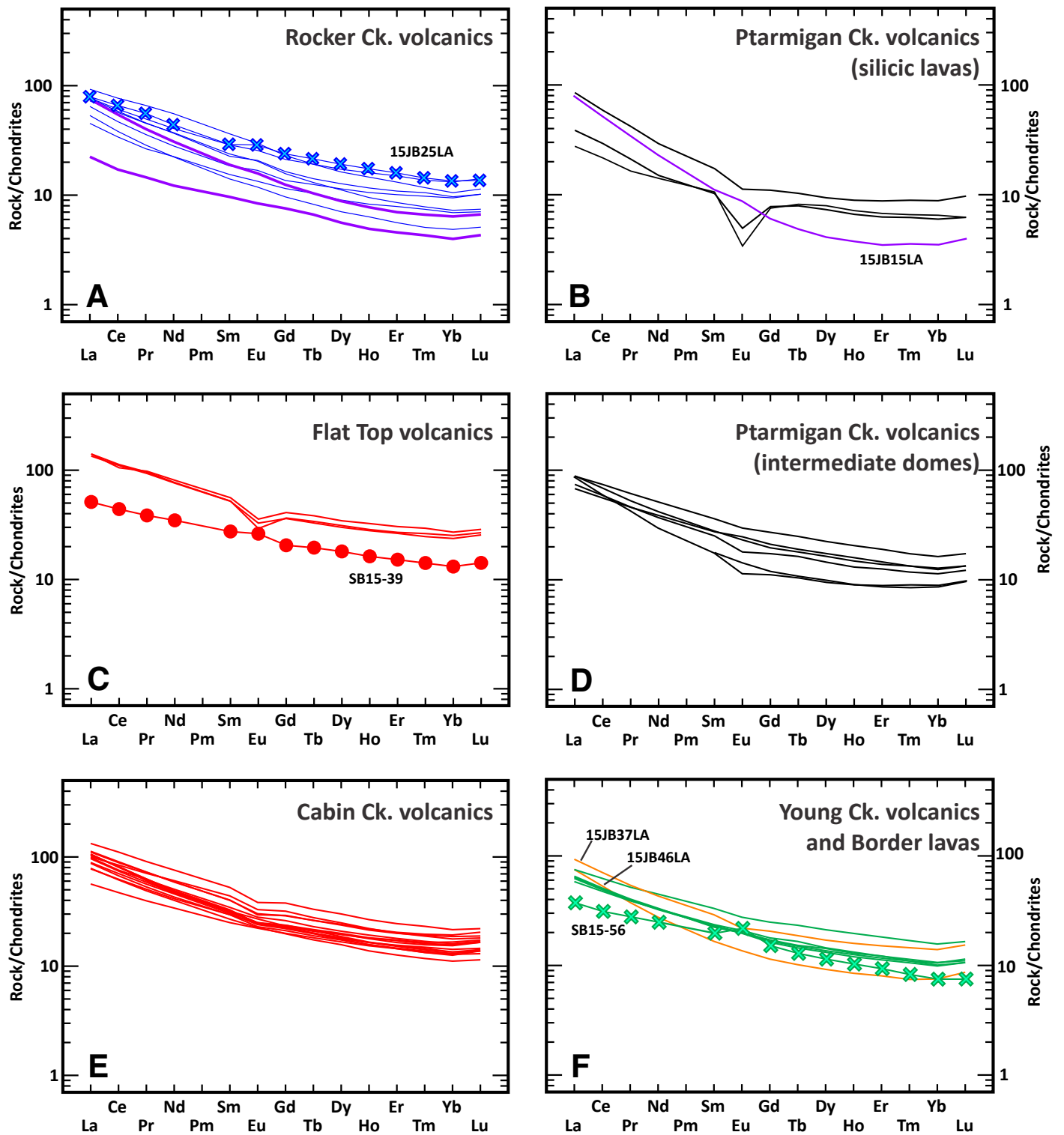


Figure 10. Chondrite-normalized, rare-earth element (REE) plots. Modified from Sun and McDonough (1989). Symbols defined in Figure 5.

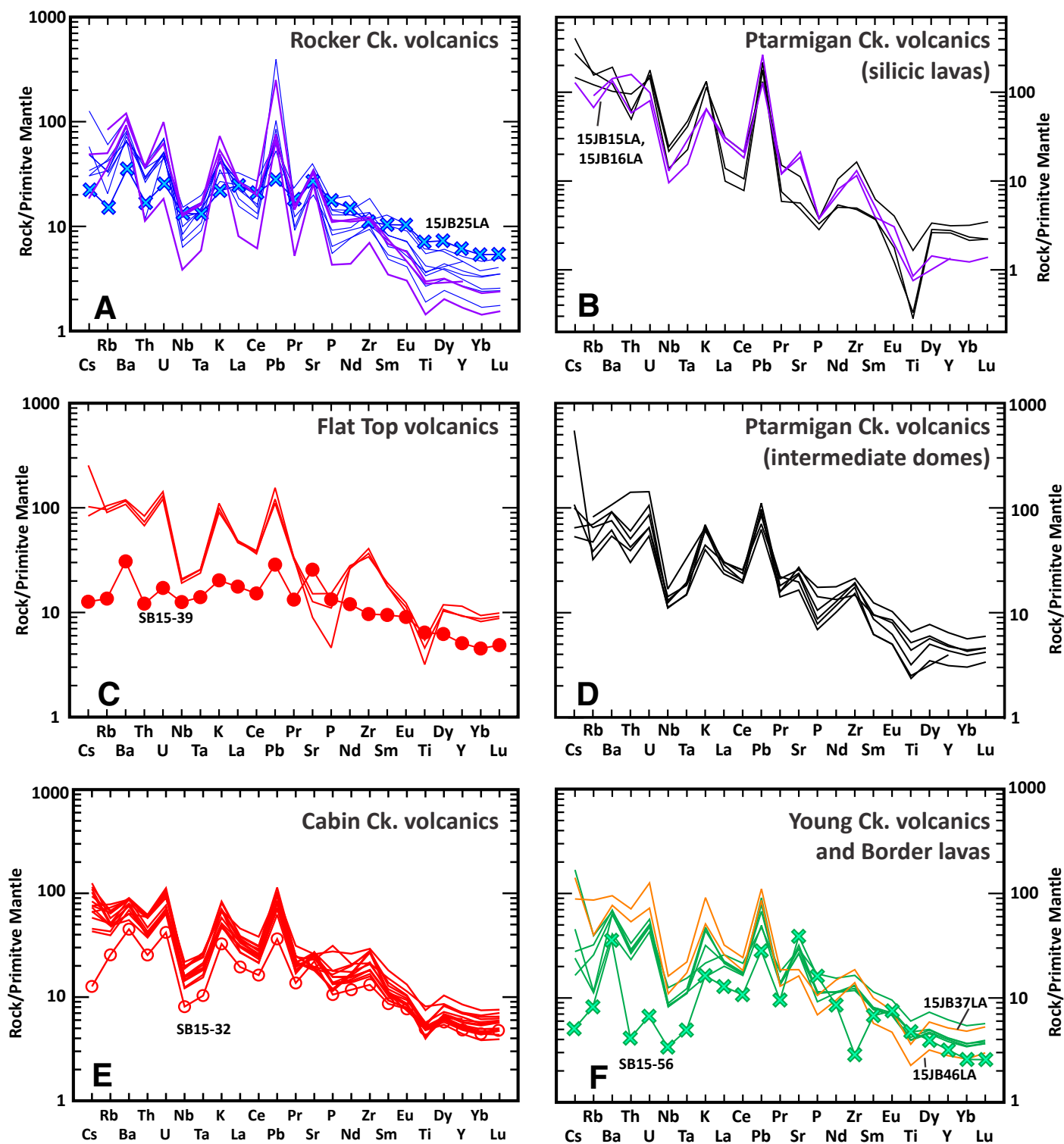


Figure 11. Primitive-mantle-normalized multi-element variation diagrams. Note the change in y-axis scale in (B) for the Ptarmigan Creek silicic lavas. Modified from Sun and McDonough (1989). Symbols defined in Figure 5.

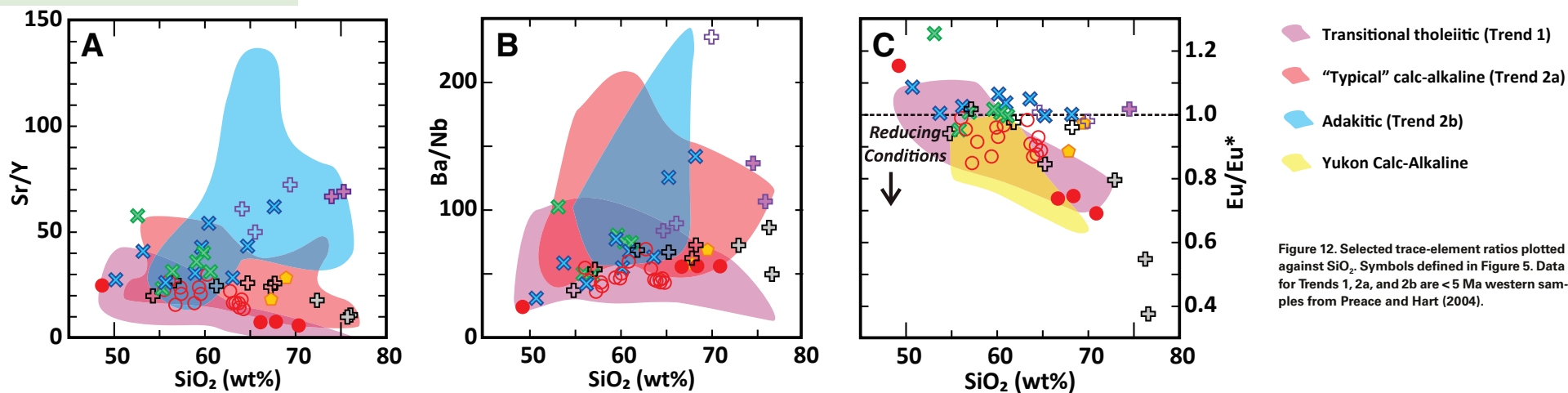


Figure 12. Selected trace-element ratios plotted against SiO_2 . Symbols defined in Figure 5. Data for Trends 1, 2a, and 2b are <5 Ma western samples from Preece and Hart (2004).

may be buried below the extensive dome field of the Ptarmigan Creek volcanics (Fig. 2). In summary, the geochemistry of the oldest volcanic rocks in the WA indicates petrogenesis under oxidizing conditions, in a subduction zone.

Ptarmigan Creek Volcanics (25–20 Ma)

Ptarmigan Creek silicic rocks show generally consistent geochemistry; LILE enrichment and HFSE depletion and the presence of hydrous phenocryst phases (biotite and/or amphibole) indicate a subduction-related origin. Sample SB15-45 is ~3–4.5 m.y. younger than the other Ptarmigan Creek silicic rocks; so it is considered separately. The remaining two silicic lavas are high-silica rhyolites and have the highest K_2O contents (>3.8 wt%) documented in the SCVF. Incompatible trace-element abundances can give information on the degree of fractionation or crustal contamination. Two silicic lavas have the highest abundances of Nb, Ta, and Rb in the SCVF (Fig. 11) and the most negative Eu anomalies (0.37–0.55, Fig. 12C). Figure 13 suggests that they follow the magma evolution path for a fractionating assemblage of plagioclase and amphibole. These two silicic lavas also have the highest Rb/Sr and lowest Zr/Nb values of the entire SCVF array, consistent with fractionation of plagioclase and zircon, respectively. Zircon was observed in these lavas; so zircon fractionation was likely responsible for the low Zr values. These trace-element data and phenocryst assemblages suggest that these two rhyolite lavas were likely generated by fractional crystallization of a hydrous parental magma, which included plagioclase, amphibole, and zircon fractionation (Drake, 1975; Drake and Weill, 1975). They erupted at 23.9–23.2 Ma, during the latest phases of Rocker Creek eruptive activity. However, the geochemical variations in Figures 8–11 suggest that the two rhyolites are more closely related to a magmatic

system similar to the intermediate domes (i.e., hydrous, subduction-related, calc-alkaline magmas without the adakite component).

The Ptarmigan Creek intermediate dome field lies between the Rocker Creek volcanics and Cabin Creek–Flat Top–Young Creek volcanics both geographically and in geochemical parameters. A wide range of geochemical compositions and a variety of petrographic textures (i.e., basaltic-andesite cumulate and intrusive diorites to rhyolitic porphyritic-extrusive lavas) exist within the sampled area. Bulk geochemistry and mineralogy (presence of hydrous phases biotite and amphibole; Fig. S2 [footnote 1]) suggest that these rocks represent typical hydrous subduction-related processes, but with slightly lower values for slab-fluid signatures than Rocker Creek lavas and domes (i.e., Sr/Y, Ba/Nb; Fig. 12). The Ptarmigan Creek intermediate dome rocks are chemically similar to trend 2a of Preece and Hart (2004) of the <5 Ma western WA (Figs. 12 and 14), as well as the central WA Frederika Formation lavas of Trop et al. (2012). Those authors attribute those magma series to melting of the mantle wedge by the addition of fluids from the subducting slab. The presence of hornblende (and biotite) as phenocryst phases is consistent with the intermediate domes following the vector of a plagioclase \pm amphibole fractionating assemblage (Fig. 13). The moderate values of trace-element ratios (Fig. 12; Sr/Y and Ba/Nb) that show elevated values of LILE and other fluid-mobile elements over HFSE and other immobile elements support the interpretation of hydrous melting of mantle wedge as the main control on intermediate dome magma genesis.

Sample SB15-45 is a calc-alkaline rhyolite with a subduction signature and has hydrous phenocryst phases (biotite and amphibole), suggesting a subduction-related origin. It is similar in age (20.3 ± 0.12 Ma) to the Flat Top volcanics and the youngest Cabin Creek lavas (ca. 21–20 Ma) and was collected from a small plug with columnar jointing that intrudes the intermediate domes east of Ptarmigan Lake (Figs. 2 and S2 [footnote 1]). SB15-45 may be an unmapped

analog to four small rhyolitic domes and plugs mapped along the southeastern margin of the Sonya Creek shield volcano (Richter et al., 2000). The close spatial and temporal association of these domes and plugs with the Flat Top rocks suggests that the swarm of silicic domes and plugs may represent local crustal melts, silicic differentiation due to filter pressing within the Sonya Creek magma chamber, or resurgent magmatism after the Flat Top tuff eruption, during the late phases of the Sonya Creek shield volcano. The plug has Rb/Sr, Eu/Eu*, and major-element values comparable to the Flat Top trachydacite lavas and the Flat Top tuff, indicating a similar degree of magmatic differentiation between the two rock groups. However, the plug has hydrous phenocrysts and lacks the elevated values of HFSE and REE in the Flat Top volcanics (Figs. 10 and 11). Figure 13 shows the plug following the fractionation vector of plagioclase \pm amphibole, which is distinctly different from the silicic Flat Top volcanics. This discrepancy between the silicic rocks of similar ages suggests a difference in petrogenesis. If this silicic plug is similar in age and geochemistry to plugs mapped by Richter et al. (2000) along the southeast margin of the Sonya Creek shield volcano, these plugs represent a pulse of calc-alkaline magmatism during the late phases of SCVF activity and could potentially be related to the Young Creek and/or Border lava magmatic systems to the south.

Sonya Creek Shield Volcano: Cabin Creek and Flat Top Volcanics (25–19 Ma)

The largest volcanic feature of the SCVF is the Sonya Creek shield volcano, which has had much of its edifice removed by erosion. The Sonya Creek shield volcano is composed of a >1-km-thick succession of basaltic to rhyolitic lavas, including an obsidian-bearing unit, termed the Cabin Creek lavas after the valley in which they were sampled (Fig. 2). Bulk geochemistry shows the Cabin Creek lavas (and broadly similar Flat Top volcanics) have elevated levels of HFSE at a given SiO₂ content relative to the rest of the SCVF rocks, and they plot within the fields for trend 1 rocks of Preece and Hart (2004). Cabin Creek and Flat Top volcanics are also chemically similar to the “calc-alkaline” data from the Canada WVB volcanic fields (yellow fields in Figs. 8, 9, and 12; Skulski et al., 1991, 1992), which are interpreted to represent an input of subduction-related fluids into overlying mantle (Skulski et al., 1991, 1992). These melts would have formed in dry and reducing conditions, which resulted in the lower abundances of LILE and greater abundances of HFSE seen in geochemical variations of Cabin Creek and Flat Top volcanics (Figs. 8 and 9). Melting of this kind could be triggered by extensional pressure release (decompression melting) rather than flux-melting of the mantle wedge (Preece and Hart, 2004). Eu/Eu* values of Cabin Creek and Flat Top volcanics (0.69–0.99; excluding the Flat Top basalt, SB15-39) suggest that these magmas formed under relatively reducing conditions, allowing Eu²⁺ to partition into plagioclase as a fractionating phase (Fig. 12D; Drake, 1975; Drake and Weill, 1975). Figure 14A shows the Cabin Creek and Flat Top volcanics plot along the vector of a plagioclase \pm olivine \pm pyroxene (\pm magnetite) fractionating assemblage, consistent with observed mineralogy.

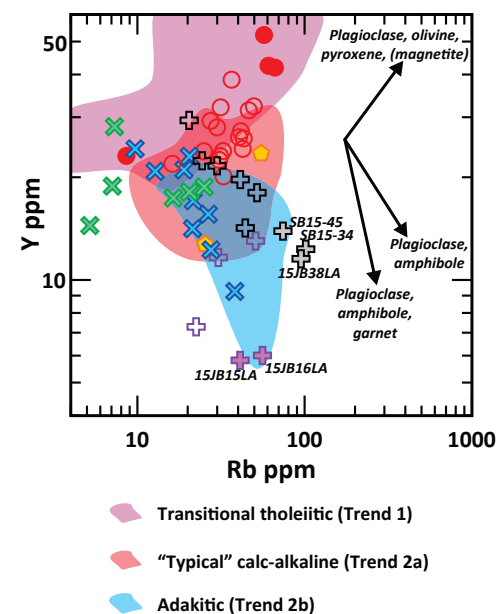


Figure 13. Y versus Rb discrimination diagram, showing the vectors for various fractionating and/or residual assemblage assemblages. Colored fields are for trends 1 (green), 2a (blue), and 2b (red) of <5 Ma Wrangell Arc (WA) rocks (Preece and Hart, 2004). Symbols defined in Figure 5.

Flat Top trachydacite lavas and the Flat Top tuff crop out topographically higher than the adjacent Cabin Creek lavas, are younger than the bulk of Cabin Creek lavas, and lie along the same geochemical arrays to high SiO₂ values, suggesting these rocks may be part of the same volcanic system (Figs. 8, 9, and 12). This interpretation is consistent with Richter et al.'s (2000) mapping, which shows fracture-associated domes, plugs, dikes, and lava flows along the northeast margin of the SC shield (Fig. 2). The basalt sampled from low in the Flat Top stratigraphy (SB15-39) is ~5.3 m.y. older than the overlying trachydacites and rhyolite and is compositionally distinct (Figs. 8, 9, and 11). The age of the Flat Top basalt (24.6 \pm 0.3 Ma) falls within the error for the Rocker Creek basalt (15JB25LA; 25.5 \pm 2.9 Ma). This relationship likely suggests that the only two basalts sampled from the SCVF may represent the same mafic pulse of magmatism into the system.

Young Creek Volcanics and Border Lavas (23–19 Ma)

The Young Creek volcanics generally overlap with trend 2a data of Preece and Hart (2004) (Figs. 8, 9, and 12). Those authors interpret that trend as

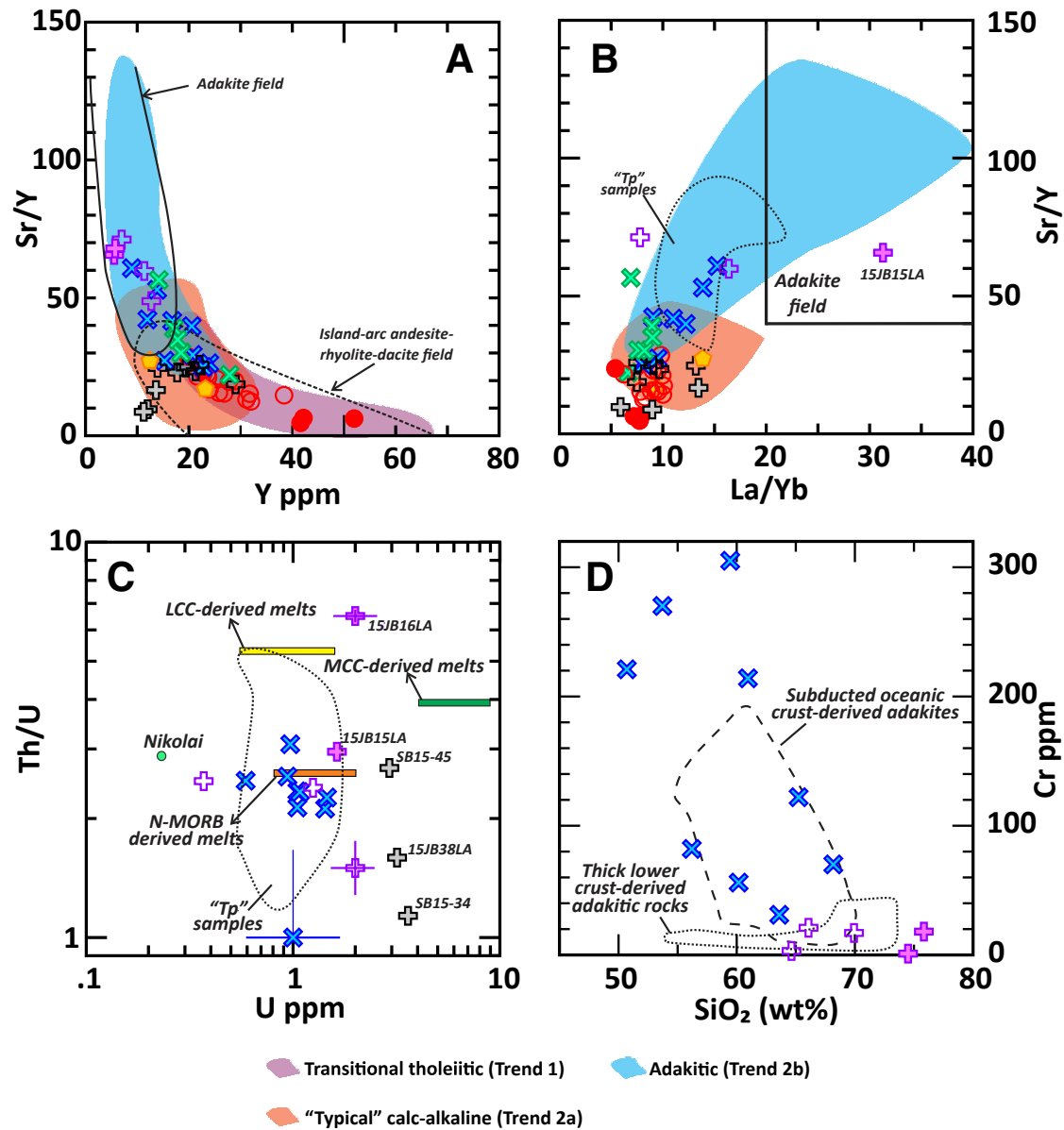


Figure 14. (A) Sr/Y versus Y plot after Defant et al. (1991), showing the fields for adakites and island-arc andesite-rhyolite-dacites. Colored fields for <5 Ma Wrangell Arc (WA) rock types are the same as in previous diagrams. (B) Sr/Y versus La/Yb plot showing the adakite field. Trend 2b andesites and transitional dacites (Preece and Hart, 2004) have adakitic Sr/Y, Sr, and Y contents, but more moderate rare-earth element (REE) characteristics. Hypabyssal "Tp" samples from the northern flank of the WA plot within the field marked by the dotted line; refer to Figure 1A for outcrop extent of Tp intrusives. (C) Th/U versus U plot after Karsli et al. (2011), showing fields for normal mid-ocean ridge basalt (N-MORB) (Sun et al., 2008) and lower and middle continental crust (LCC, MCC; Rudnick and Gao, 2003). Nikolai Greenstone data are from Greene et al. (2008, 2009). Error bars are one standard deviation for X-ray fluorescence trace element data. (D) Cr versus SiO₂ variations of Rocker and Ptarmigan Creek volcanics, including adakite-like rocks. Fields for subducted oceanic-crust-derived adakites, and thick lower-crust-derived adakitic rocks are from Wang et al. (2006) and references therein. Symbols defined in Figure 5.

reflecting “typical” subduction-related geochemical affinities, with enrichments in LILE and depletions in HFSE (Fig. 11). The Young Creek lavas erupted during the latest phases of SCVF volcanic activity (19.1–19.3 Ma) from an unknown source in the southwest segment of the volcanic field (Fig. 2; Table 1). The mafic diorite from Rock Lake (22.9 ± 2.2 Ma) is included in this group based on chemistry and age data and may represent a sub-volcanic root of an eruptive source for the Young Creek rocks (Figs. 2 and 4; Table 1). Our new geochronological data show that the Young Creek rocks overlap in age with the youngest phases of Cabin Creek and Flat Top magmatism (Fig. 3; Table 1); this overlap contradicts the interpretation of Richter et al. (2000) that Young Creek rocks are at least 23 Ma. However, field relations show flat-lying Flat Top rocks that overlie tilted Young Creek rocks (Figs. 2 and 4), indicating that the exact relationship between this geographically close magmatism is complicated and may be overlapping in places.

The sampled Border lavas have typical subduction-related chemistry and are generally chemically similar to Young Creek rocks, but at higher SiO₂ values (Figs. 8 and 9). The Border lavas overlap in age with the Young Creek rocks, and although they are more silicic than the Young Creek volcanics, those two rocks groups show similar geochemical profiles (Figs. 10 and 11). This relationship does not imply that the Border lavas and Young Creek volcanics are petrogenetically related, but the close association in time and space, and their geochemical similarity, indicate that the two rock groups may have formed from a similar subduction-related magmatic event that erupted via different volcanoes. Regardless, the Border lavas and Young Creek rocks represent a shift to calc-alkaline magmatism in a southward direction, away from the Sonya Creek shield volcano. The alkaline to calc-alkaline St. Clare Creek volcanic field in Yukon Territory (~80 km to the southeast; SC on Fig. 1) was active immediately following SCVF activity at ca. 18 Ma (Skulski et al., 1992), and Young Creek and Border lava magmatism represents the beginning of this southward shift.

Adakite-Like Signature in Rocker Creek and Ptarmigan Creek Volcanics

Some Rocker Creek and Ptarmigan Creek volcanic rocks have higher Sr/Y values than most other SCVF rocks (Fig. 14A); these values imply a role for garnet or amphibole in the source rock (Defant et al., 1991). Figure 13 shows that the differentiation array of these rocks could be controlled by a fractionating and/or residual assemblage of plagioclase ± amphibole ± garnet. These rocks do not have the high La/Yb values (>20) that would suggest a strong role for residual garnet, which is inconsistent with the formal usage of the term “adakite” as defined by Defant and Drummond (1990) (Figs. 14A and 14B). However, these rocks are chemically similar to the Mount Drum “transitional” dacites and andesites of the trend 2b adakite suite of Preece and Hart (2004); this suite consists of adakite-like Sr, Y, and Sr/Y, but slightly lower La/Yb ratios than adakites *sensu stricto* (Castillo, 2012; Fig. 14B). Those rocks plot between the adakite field and the evolved arc-related rocks of trends 1 and 2a, which

we interpret to represent mixing between an adakite-like melt (slab melt or mafic lower-crustal melt) and some other primitive magma derived from a subduction-fluxed mantle wedge (Preece and Hart, 2004).

Geochemical and geochronological data reported recently from hypabyssal hornblende dacite intrusions ~60–100 km northwest of the SCVF documents adakite-like magmatism from ca. 29–22 Ma along the northern flank of the WA (data shown in dashed field in Fig. 14C; Weber et al., 2017). The two Ptarmigan Creek high-Si adakites (15JB15LA and 15JB16LA) have high Sr/Y (15JB15LA has high La/Yb) and may represent a differentiated product of an adakite-like magma that formed via melting of a slab edge or lower crust during subduction initiation (Defant and Drummond, 1990; Sajona et al., 1993; Peacock et al., 1994) and then underwent mixing with another primitive mantle-wedge melt to produce the geochemical array of the Rocker Creek volcanics. These two Ptarmigan Creek adakites have Nb and Ta values that are equal to, and in some cases, lower than, the Rocker Creek volcanics. Because Nb and Ta are incompatible in mafic minerals (Gill, 2010), the low values of those elements in the two rhyolites are not likely to result from differentiation of a mafic magma by fractional crystallization. Additionally, the two adakite-like samples have Eu/Eu* values close to one (Fig. 12C) and low Rb/Sr values, suggesting that plagioclase fractionation was not an important process in magma evolution. Although these two lavas share other major- and trace-element characteristics with the Ptarmigan Creek volcanics (discussed below), they likely belong to another eruptive system.

Trace elements for SCVF adakite-like rocks can be used to distinguish between melting of the slab and the lower crust, in lieu of radiogenic isotope data. A plot of Th/U versus U (Fig. 14C) shows that one of the Ptarmigan Creek adakites plots close to the fields for melts derived from middle continental crust and lower continental crust (Rudnick and Gao, 2003; Karsli et al., 2011), even considering the larger uncertainty for this XRF data (Fig. 14C). However, the other adakite lava (15JB15LA) plots close to the field for N-MORB-derived melts, along with the Rocker Creek volcanics. This could be evidence that the two Ptarmigan Creek adakite-like silicic lavas are not petrogenetically related, or secondary alteration by surface processes has changed the values of the fluid-mobile trace elements, U or Th. Regardless, the U and Th element data suggest some amount of lower- to middle-crust involvement in the generation of at least one of the adakite-like rhyolites. Figure 13A shows that the two silicic adakite-like lavas follow the vectors of a fractionating and/or residual assemblage containing amphibole ± garnet, as opposed to the Ptarmigan Creek intermediate rocks (Pearce and Norry, 1979; Irving and Frey, 1984).

Figure 14C shows the Rocker Creek volcanics plot near the field for N-MORB-derived melts. So, if they were derived from a mafic lower-crustal rock, it would have to be more similar to an underplated basalt in composition (more primitive) than global average lower continental crust (Fig. 14C; Rudnick and Gao, 2003). The Rocker Creek volcanics have Mg#, MgO, Ni, and Cr values (Figs. 8, 9, and 14D) that suggest interaction with mantle-wedge peridotite and therefore either derivation by melting of delaminated mafic lower crust or melting of subducted oceanic basalt. Cretaceous adakitic andesites and dacites from

China have been demonstrated to form via delamination of underplated mafic lower crust that sank into the mantle, equilibrated with mantle peridotite, and partially melted (Xu et al., 2002; Wang et al., 2006). However, Rocker Creek volcanics extend to more primitive compositions (six samples with $\text{SiO}_2 < 63$ wt%) and have higher MgO, Cr, and Ni values at a given SiO_2 content than the Chinese adakites (Fig. 14D; Xu et al., 2002). The MgO, Ni, and Cr values for the majority of SCVF adakite-like rocks strongly suggest that their adakite-like signature was not derived via melting of mafic lower crust. A direct melt of the subducted Yakutat slab during subduction initiation is more likely as the source of the adakite-like signature in the SCVF and along the northern flank of the WA. Adakite chemistries have been shown to form via a number of geological processes in addition to slab melting (Castillo, 2012), and studies of arc magmatism also often associate adakites with high-Mg andesites (Mg# 45, wt% $\text{SiO}_2 = 54\%–65\%$; Grove et al., 2003; Kelemen et al., 2003; Streck and Leeman, 2018), rocks which have controversial (e.g., primitive melts of mantle-wedge versus magma-mixing) origins. However, slab melting does appear to be a viable process to form WA adakite-like magmas, especially when the subducting slab is young, shallow-dipping, and at shallow depths (Yogodzinski et al., 1995, 2001; Drummond et al., 1996; Gutscher et al., 2000). These conditions characterize southern Alaska and have done so for at least the past ~30 m.y. (Ferris et al., 2003; Finzel et al., 2011, 2016; Brueseke et al., 2019).

The tectonic implications of our data are the following: melting of either the slab-edge itself or mafic lower crust was triggered by mantle flow around the leading or lateral edge of the slab following the initiation of subduction of the Yakutat oceanic crust (Fig. 15). Recent three-dimensional modeling shows that toroidal flow of warm sub-slab mantle around the lateral edge of the Yakutat slab may have occurred (Jadamec, 2016). This upwelling sub-slab mantle could induce melting of the slab-edge or lower crust, with both melt sources

giving rise to adakite-like magmas, and is consistent with recent geophysical study of south-central Alaska subduction that suggests that the modern WA exists above the Yakutat slab edge (Martin-Short et al., 2018). Preece and Hart (2004) proposed a slab-edge melting scenario of slab heating for < 1 Ma WA adakites that erupted from Mount Churchill, partially due to the slowing of subduction rate. This interpretation is in line with recent geophysical constraints that indicate the WA trench has become more of a collisional zone in the past ~1 m.y. (Gulick et al., 2013). Preece and Hart (2004) and Thorkelson et al. (2011) proposed a slab-window scenario of adakite production in the WA. We propose a modified model for the presence of ca. 30–23 Ma WA adakite magmas: slab-edge melting due to toroidal flow during rapid convergence between the Yakutat microplate and North America.

REGIONAL ARC-TRANSFORM TECTONIC IMPLICATIONS

Wrangell Arc Initiation: Yakutat Subduction and Changes in Relative Plate Motion

New field, geochemical, and geochronological data for the Oligo–Miocene Sonya Creek volcanic field place constraints on the tectonic history during initiation of the Wrangell Arc starting ca. 30 Ma (Figs. 3 and 16). Initial emplacement of subduction-related calc-alkaline magmas, including some with adakite-like chemistry, was followed by a geochemical, temporal, and geographic shift to more transitional-tholeiitic affinities related to anhydrous melting due to intra-arc extension. An additional pulse of calc-alkaline magmatism marked the end of SCVF activity. SCVF geochemical compositions are broadly similar to those documented in the central and western WA (ca. 12 Ma–Holocene),

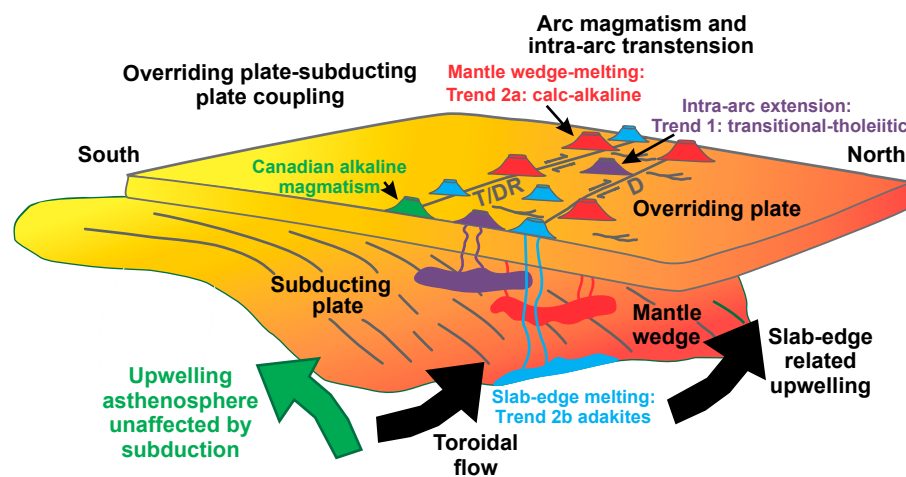


Figure 15. Three-dimensional cartoon (adapted from Jadamec, 2016) depicting the Wrangell volcanic belt (WVB), illustrating subduction of the Yakutat slab, melt source regions for WVB magmas (after Skulski et al., 1991; Edwards and Russell, 2000; Preece and Hart 2004; Thorkelson et al., 2011; Trop et al., 2012; Brueseke et al., 2019; this study), and major upper-plate strike-slip faults. T/DR – Totschunda/Duke River fault.

reflecting the dominant roles of subduction and intra-arc extension on magma production. Exceptions are the presence of adakite-like lavas (trend 2b) and the lack of alkaline magmatism that characterized <19 Ma volcanism in adjacent areas of Yukon. Trend 2b rocks have not been identified in the older than <5 Ma Wrangell Arc until recently (Morter et al., 2016; Brueseke et al., 2019; this study). We propose a model for the geochemical changes documented in the SCVF, where a change in subduction angle or convergence angle and/or rate initiated melting of previously modified and/or enriched MORB mantle. An initial geochemical signature of typical subduction-related calc-alkaline affinities (trend 2a; Rocker and Ptarmigan Creek volcanics) gave way to more transitional-tholeiitic affinities (trend 1; Cabin Creek and/or Flat Top), followed by a return to typical calc-alkaline magmatism (trend 2a; Young Creek and Border lavas). All three phases of SCVF magmatism are consistent with the subduction of the initial thinner edge of the Yakutat microplate or, alternatively, subduction of “typical” thickness oceanic crust in front of the Yakutat microplate. The latter is consistent with geophysical studies and modeling that imply the subducting Yakutat microplate plays a role in WA magmatism and the lack of any anomalous geochemical changes in erupted volcanic products during the ~30 m.y. duration of the WA (Jadamec and Billen, 2010, 2012; Bauer et al., 2014; Martin-Short et al., 2016; Wech, 2016; Martin-Short et al., 2018; Brueseke et al., 2019; Pavlis et al., 2019; Venereau et al., 2019).

Our new geochemical and geochronological data document initiation of the Wrangell Arc ca. 30 Ma along the inboard margin of the subducted Yakutat microplate. The timing of arc initiation is consistent with thermochronologic and stratigraphic records reported previously from the region above and adjacent to the Yakutat flat slab. Collectively, these studies document upper-plate processes attributable to flat-slab subduction starting in late Oligocene time, including shortening, exhumation, and erosion of the upper plate, shoaling or inversion of sedimentary basins above the flat-slab region, and deposition of thick, clastic wedges in sedimentary basins located along the western and northern perimeters of the flat-slab region (Berger et al., 2008a, 2008b; Enkelmann et al., 2008, 2010; McAleer et al., 2009; Finzel et al., 2011, 2016; Arkle et al., 2013; Grabowski et al., 2013; Falkowski et al., 2014, 2016; Falkowski and Enkelmann, 2016; Dunn et al., 2017; Enkelmann et al., 2017).

The overall frequency of SCVF magmatism appears to reflect not only the initiation of Yakutat flat-slab subduction (Benowitz et al., 2014; Lease et al., 2016) but also a newly defined change in Pacific plate direction and velocity at ca. 25 Ma (Jicha et al., 2018) (Figs. 3 and 16). The initiation of Yakutat flat-slab subduction is associated with the shutting off of arc magmatism in the Alaska Range (Trop et al., 2019), basin subsidence and inversion (Ridgway et al., 2012), and deformation across southern Alaska (e.g., Lease et al., 2016). The initiation of the Wrangell Arc has also been linked with initiation of Yakutat flat-slab subduction (Richter et al., 1990; Brueseke et al., 2019; this study). Jicha et al. (2018), based on a kink in the northwest Hawaiian Ridge, defined a change in Pacific direction (more northerly) and velocity (52% increase) at 25.3 Ma \pm 0.5 Ma. The authors noted numerous tectonic and volcanic events at this time across the circum-Pacific, including an increase in deformation

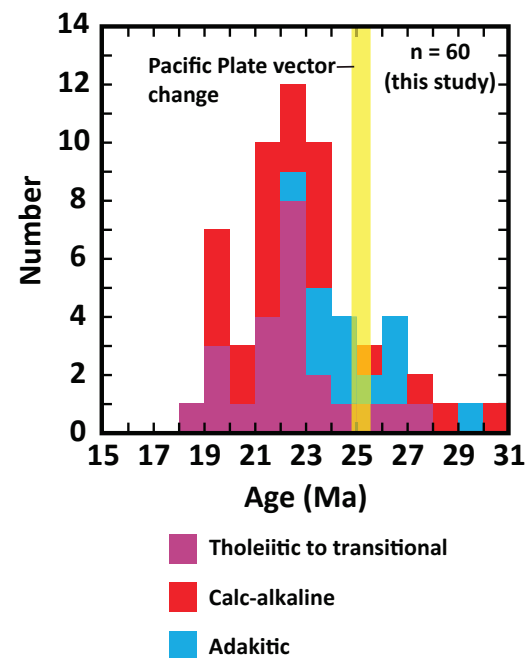


Figure 16. Histogram of Sonya Creek volcanic field igneous ages, where magmatism is also divided by geochemistry (e.g., trend 1—transitional-tholeiitic; trend 2a—calc-alkaline; trend 2b—adakite). Note the increase in magmatism ca. 25 Ma, which also corresponds to an increase in convergence rate of the Pacific-Yakutat plate at ca. 25 Ma with Alaska documented by Jicha et al. (2018).

rates across the entirety of the Alaska Range (see Benowitz et al., 2014, for a summary). Based on our new geochronology and geochemistry data (Figs. 3 and 16), the SCVF appears to have experienced an increase in magmatic flux and potentially an increase in slab-edge melting (e.g., adakite generation) at ca. 25 Ma; this melting aligns well with the previously identified ca. 25 Ma southern Alaska tectonic event (Benowitz et al., 2014). This new interpretation of the plate boundary driver for ca. 25 Ma deformation events across southern Alaska helps reconcile the apparent conflict of the initiation of Yakutat flat-slab subduction (ca. 42–32 Ma, Finzel et al., 2011; ca. 30 Ma, Brueseke et al., 2019) >5 m.y. prior to enhanced deformation across southern Alaska ca. 25 Ma (Benowitz et al., 2012a; Benowitz et al., 2014).

We suggest that increased convergence rates can lead to more torpid mantle flow and could explain the apparent increase in adakite-like magmatism after the ca. 25 Ma change in Pacific plate vector. This scenario may explain WA adakite magmatism ca. 5 Ma to ca. 3 Ma, which has been attributed to a slab window (Preece and Hart, 2004; Thorkelson et al., 2011). Circa 5 Ma is also

when the known change in Pacific plate vector became more convergent with Alaska and also more rapid (Engbretson et al., 1985). This change has been linked to late Miocene deformation in the Alaska Range (Waldien et al., 2018).

Our new geochemical and geochronological data also indicate that an increase in convergence rate of the Pacific-Yakutat plate at ca. 25 Ma with Alaska (Jicha et al., 2018) may have transferred some component of strain to the upper plate via the Denali-Totschunda fault system ca. 23–22 Ma, based on the initiation of transitional-tholeiitic Sonya Creek shield volcanism (Fig. 16). This inference aligns well with known constraints on slip rates along the Denali fault system (Benowitz et al., 2012b). Immediately following SCVF magmatism, primitive alkaline lavas erupted to the southeast along the Duke River fault in the Yukon from ca. 18–16 Ma (Skulski et al., 1991, 1992). Extensional stresses across strike-slip faults (i.e., transtension) facilitate the ascent of mantle melts (Takada, 1994), and changes in degree of partial melting would result in variations in geochemistry (Preece and Hart, 2004). Our interpretation is that the presence of a subduction-modified mantle wedge would impart the trace-element subduction signature on transitional to calc-alkaline magmas, similar to what is documented in the “calc-alkaline” rocks from the eastern WVB in Canada. Dextral strike-slip motion documented along the Denali, Totschunda, and/or Duke River faults (Ridgway and DeCelles, 1993; Matmon et al., 2006; Cobbett et al., 2017) would be expected to shift the position of arc volcanoes southward and provide conduits for magma ascent (Skulski et al., 1991, 1992). Transtensional tectonics persisted throughout development of the WA, including ca. 12–8 Ma transtensional arc volcanism and intra-arc basin development in the central WA (Trop et al., 2012) and Quaternary transtensional intra-arc magmatism in the western WA (Preece and Hart, 2004). This >30 Ma record of transtensional tectonics highlights the importance of both arc magmatism and strike-slip deformation in the complex transition zone of arc-transform margins.

Original Extent and Postemplacement Lateral Shuffling of the Wrangell Arc

The location of the SCVF, as well as that of geochemically and temporally similar ca. 30–20 Ma hypabyssal rocks from the northern flank of the modern WA, designate the position of the WA at its initiation (Weber et al., 2017). These hypabyssal rocks and the SCVF define a <100-km-long, northwest-trending outcrop belt that is displaced by the Totschunda fault (Figs. 1 and 17). Recent studies document Late Cenozoic offset along the Totschunda fault, but its overall offset history is not well established (Haeussler et al., 2017; Marechal et al., 2018). We infer that the SCVF and the coeval plutonic rocks were originally contiguous and thus constrain total possible lateral offset along the Totschunda fault. Based on this interpretation, the maximum amount of dextral displacement since ca. 18 Ma (age of the youngest pulse of magmatism in the displaced outcrop belt) is <85 km (Fig. 17). We acknowledge that it is possible that yet unsampled similarly aged rocks exist in this region and, depending on where they crop out, could change displacement calculations. However, U/Pb geochronology of

detrital zircons and $^{40}\text{Ar}/^{39}\text{Ar}$ geochronology of sand- and gravel-sized volcanic clasts from modern rivers encircling the WA reveal only a handful of 30–40 Ma grains (<1% of >1600 new ages), followed by continuous magmatism from ca. 30 Ma to present (Davis et al., 2017; Trop et al., 2018). Waldien et al. (2018), based on lithofacies analysis and the timing of thrust belt initiation along the Denali fault system, inferred the Totschunda fault experienced a maximum of ~80 km of offset since ca. 6 Ma, which aligns well with our new estimate of ~85 km of dextral slip along the Totschunda fault since ca. 18 Ma.

The shift of volcanic locus from the SCVF to the Yukon volcanic fields at ca. 18 Ma represents a southeastward shift of magmatism during the early phases of the WA. Continued northwestward migration of magmatism, from ca. 18 Ma onward, is documented by other studies of the WA igneous and sedimentary bedrock record (e.g., Richter et al., 1990; Preece and Hart, 2004; Trop et al., 2012) and thermochronologic data that document exhumation in the central WA ca. 5–4 Ma (Enkelmann et al., 2010). An exception to the northwestward-younging pattern of volcanism is Mount Churchill, a Holocene stratovolcano in the central WA that erupted large-volume (VEI [volcanic explosivity index] = 6, White River ash) silicic fall deposits as recently as 1147 yr B.P. (Clague et al., 1995; Preece et al., 2014). Northwestward migration of magmatism and associated intra-arc extension and/or basin development has been attributed to the progressive northwestward insertion of the northwestward-tapering Yakutat slab (Worthington et al., 2012) into the continental margin of south-central Alaska synchronous with a documented change in plate motion (Richter et al., 1990; Preece and Hart, 2004; Trop et al., 2012). Subduction-related fluids were derived from the shallow Yakutat slab, which initiated flux melting of the mantle wedge below the modern WA (Brueseke et al., 2019). Transitional-tholeiitic eruptive products, aligned cinder cones, and sedimentary basins in the interior of the WA suggest an intra-arc extensional regime (Lunt, 1997; Trop et al., 2012). Localized intra-arc basin development and volcanism were likely accommodated by extensional deformation along documented north-striking normal faults and, more speculatively, transtensional basin development associated with northwest-striking, right-lateral, strike-slip faults, including the Totschunda fault (Fig. 1; Trop et al., 2012). Adakite dacite lavas from Mounts Drum and Churchill reflect Holocene melting of the Yakutat slab (Preece and Hart, 2004; Preece et al., 2014).

■ COMPARISONS TO GLOBAL ARC-TRANSFORM SETTINGS

The temporal, geochemical, and geographic shifts observed in the Sonya Creek volcanic field have implications for continental arc-transform junctions worldwide and throughout Earth history. Geochemistry of magmatic products in these transition zones are sensitive to slight shifts in the relative position of the subducting and overriding plates, as well as changes in rate and direction of convergence, angle of subduction, and motion along strike-slip faults (Park et al., 2002; Maury et al., 2004; Portnyagin et al., 2005; Tibaldi et al., 2010; Lee et al., 2016). The presence of heterogeneous mantle materials introduces additional

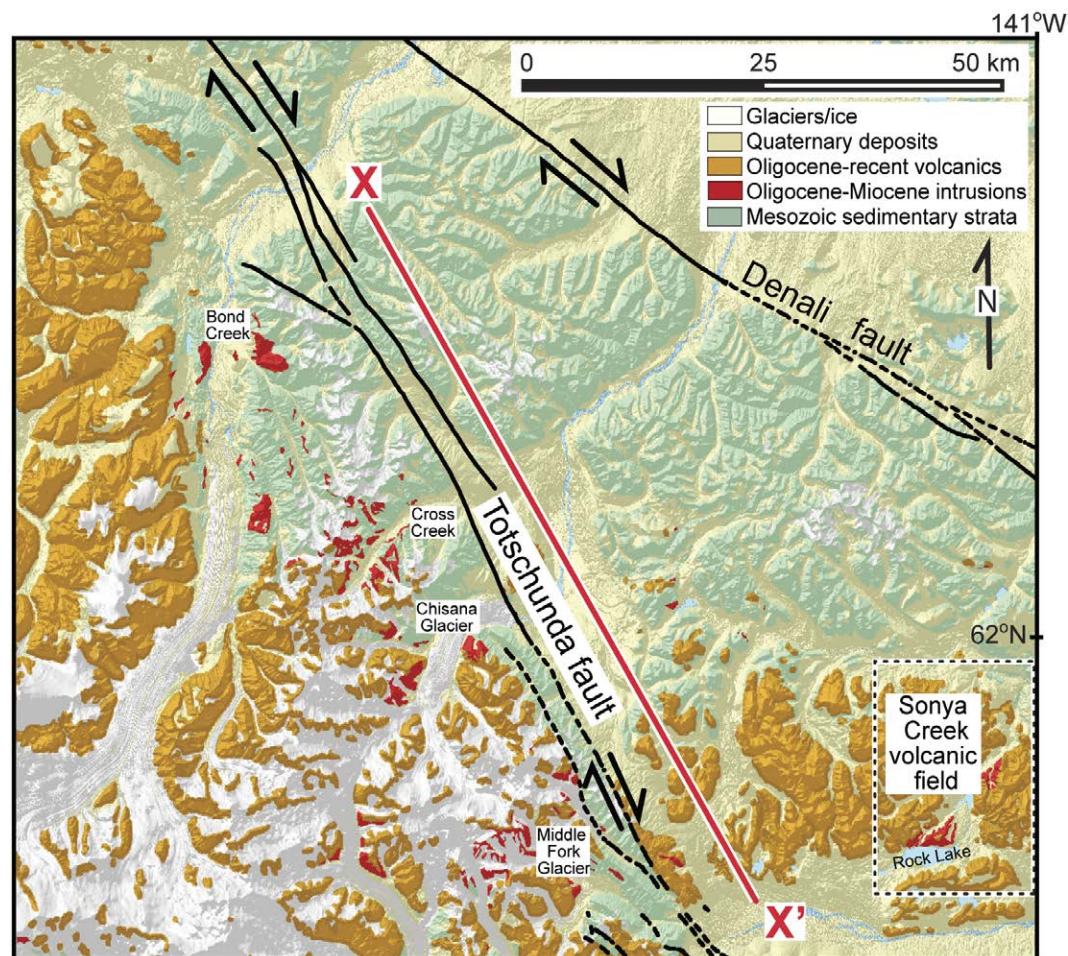


Figure 17. Geologic map showing intrusions (red) that overlap the age range of ca. 20–30 Ma volcanic and intrusive rocks in the Sonya Creek volcanic field (this study). Assuming the coeval intrusions and Sonya Creek volcanics were initially part of the same magmatic episode, the maximum amount of dextral displacement along the Totschunda fault since 25 Ma is <80 km (length of red line X–X' is ~80 km).

complications, because changes in tectonic configuration can cause mantle flow and inheritance of previous geochemical signatures. An along-strike transition to oblique and strike-slip motion is ubiquitous in convergent margins, and understanding the geochemical signature of magmatic initiation can help to recognize similar situations in the geologic record, especially in arc-transform zones that are characterized by both arc magmatism and strike-slip deformation.

As discussed earlier, the geochemistry of arc-transform volcanic systems exhibits considerable variability beyond the calc-alkaline signature typical of subduction and/or arc processes. A significant geochemical aspect of the SCVF (as well as the modern WA) is the presence of transitional-tholeiitic magma series, interpreted here and by other workers to represent mantle-wedge

melting associated with intra-arc extension, in this case, associated with coeval transtension along major strike-slip faults. Anomalous geochemical signatures are characteristic of arc-transform transition zones, and the presence of adakite-like affinities has tectonic significance. The presence of SCVF rocks with elevated Sr/Y (20–70), and one sample with elevated La/Yb (~20), as well as the SiO₂ versus Cr relations (Fig. 14D), suggests the role of an adakitic component in magma genesis (Fig. 15). The most likely mechanisms in the WA for adakite generation are the upwelling, thermal ablation, and melting of the Yakutat slab (Preece and Hart, 2004; Jadamec and Billen, 2010; Martin-Short et al., 2018; Brueseke et al., 2019). At least one of the adakite-like silicic lavas in the SCVF (15JB16LA) may have originated via melting of some mafic lower-crustal rock,

but the MgO, Ni, and Cr values of the Rocker Creek lavas and domes indicate that they more closely resemble adakites derived from slab melting, rather than melting of thick mafic lower crust (Figs. 14C and 14D). The higher Mg, Ni, and Cr concentrations in slab-melt-derived adakite-like magmas are suggested to derive from the melt reacting with mantle-wedge peridotite (Kepezhinskas et al., 1995; Stern and Kilian, 1996; Rapp et al., 1999; Wang et al., 2006). A similar scenario is observed where the Kamchatka arc meets the Aleutian arc at a 90° angle in the northwestern Pacific. Adakitic volcanic rocks there are interpreted to represent the melting of subducted Pacific lithosphere as sub-slab asthenosphere rises around the edge of a slab window (Yogodzinski et al., 2001; Park et al., 2002) or slab melts of eclogitic Pacific plate reacting with heterogeneous mantle wedge (Portnyagin et al., 2007). In Kamchatka, volcanism north of the subducting Pacific plate (e.g., Nachikinsky volcano, etc.) is characterized by decompression mantle melting of asthenosphere relatively unaffected by subduction (Portnyagin et al., 2007). This relationship parallels the interpretation of alkaline mafic lavas in the Canadian portions of the WVVB by Skulski et al. (1992), Thorkelson et al. (2011), and Brueseke et al. (2019)—that their geochemistry reflects a decreased subduction input and intraplate and/or slab-window melting environment, adjacent to the Yakutat slab (Fig. 15).

Cenozoic volcanism in Myanmar along the dextral Sangaing transform fault also shows chemical similarities to the SCVF. There, mid-Miocene volcanic rocks are calc-alkaline and inferred to form via typical subduction-fluid-related melting of mantle-wedge asthenosphere above the subducting Indian oceanic lithosphere (Maury et al., 2004; Lee et al., 2016). In other locations (e.g., Trans-Mexican volcanic belt and Northern Cordilleran volcanic province), changes in plate convergence rates are associated with upwelling asthenosphere leading to OIB-like alkaline magmatism and modification of the mantle wedge and slab-edge melts (adakites, *sensu stricto*) (Edwards and Russell, 2000; Lühr, 2000; Ferrari et al., 2001; Thorkelson et al., 2011). Specific volcanic geochemistry depends on the local asthenosphere and lithospheric mantle, but changes in plate motion drove magmatism hundreds of kilometers inboard of the continental margin in these locations.

CONCLUSIONS

- (1) Igneous rocks from the Sonya Creek volcanic field yield mineralogical and geochemical data that reflect calc-alkaline magmatism due to subduction and formation of a volcanic arc. In the SCVF, the 30–23 Ma Rocker Creek lavas and domes document subduction-related calc-alkaline magmatism (e.g., subduction affected mantle-wedge melting) with an apparent adakite-like component during SCVF initiation. This was followed by the emplacement of the Ptarmigan Creek volcanics, which show a temporal and spatial transition to continued subduction-related magmatism without the adakite-like component. Another geochemical and minor spatial shift is recorded by the eruption of the 25–19 Ma transitional-tholeiitic lavas of the Sonya Creek shield volcano and the

Flat Top volcanics, which indicate local intra-arc extension following arc initiation. Additional calc-alkaline magmatism, represented by the 21–19 Ma Young Creek lavas and the 21–20 Ma Border lavas, marked the end of SCVF activity. We document no evidence of alkaline magmatism that characterizes the Yukon WVVB in the SCVF.

- (2) Magmas with adakite-like affinities are documented during initiation of the WA (ca. 30–20 Ma), reflecting one or more tectonic processes that we interpret to reflect anomalous heating of the Yakutat slab and/or mafic lower crust and variable production of fluids from the descending slab. Adakite-like affinities and ages that overlap with early SCVF volcanism also characterize hypabyssal units that are exposed ~40–100 km west of the SCVF (Weber et al., 2017). These intrusions and the SCVF likely represent the early initial extent of the WA, even though the SCVF was subsequently offset laterally along the Totschunda fault.
- (3) The geochemistry and geochronology of the SCVF support existing tectonic models of southern Alaska and adjacent Yukon. Initial SCVF volcanism reflects northward and/or northeastward subduction of oceanic lithosphere of the Yakutat microplate beneath North America. A recently documented change in Pacific plate vector at ca. 25 Ma is reflected in an increase in SCVF magmatic flux and adakite magmas at that time, likely related to increased slab-edge toroidal flow due to the increase in convergence rate between the Yakutat microplate and North America.
- (4) The change in Pacific plate vector to a more northerly direction at ca. 25 Ma likely is also responsible for transferring stress to inboard strike-slip faults and initiating transtensional-related mantle melting recorded by the ca. 23–19 Ma Sonya Creek shield volcano. By ca. 18 Ma, SCVF activity ceased, and the locus of magmatism shifted to the south and east, where transtensional deformation along dextral strike-slip faults and normal faults served as conduits for “leaky transform” alkaline volcanism in adjacent parts of the Yukon.
- (5) We infer the Totschunda fault has not experienced more than 85 km of offset since ca. 18 Ma based on reconstructing the initial alignment of the SCVF to geochemically and temporally similar ca. 30–20 Ma intrusions that crop out west of the SCVF on the opposite side of the Totschunda fault.
- (6) This study of the long-lived and geochemically diverse SCVF elucidates the effects of Cenozoic northern Cordillera tectonics on the initiation of the WA specifically and more generally demonstrates the sensitivity of arc magmatic geochemistry to tectonic changes in an arc-transform transition zone.

ACKNOWLEDGMENTS

This research was part of Berkelhammer’s M.S. thesis at Kansas State. It was made possible in part by funding from National Science Foundation to Brueseke (grant EAR-1450689), Benowitz and Layer (grant EAR-1450730), and Trop (grant EAR-1450687). Publication of this article was funded in part by the Kansas State University Open Access Publishing Fund. We thank everyone at Devil’s Mountain Lodge for field and air support and National Park Service personnel at Wrangell–St. Elias

National Park and Preserve for assistance. We also thank Guest Associate Editor David Scholl and two anonymous reviewers for their constructive feedback.

REFERENCES CITED

- Arkle, J.C., Armstrong, P.A., Haeussler, P.J., Prior, M.G., Hartman, S., Sendziak, K.L., and Brush, J.A., 2013, Focused exhumation in the syntaxis of the western Chugach Mountains and Prince William Sound, Alaska: *Geological Society of America Bulletin*, v. 125, p. 776–793, <https://doi.org/10.1130/B30738.1>.
- Bai, H., and Montési, L.G.J., 2015, Slip-rate-dependent melt extraction at oceanic transform faults: *Geochemistry, Geophysics, Geosystems*, v. 16, no. 2, p. 401–419, <https://doi.org/10.1002/2014GC005579>.
- Bauer, M.A., Pavlis, G.L., and Landes, M., 2014, Subduction geometry of the Yakutat terrane, southeastern Alaska: *Geosphere*, v. 10, no. 6, p. 1161–1176, <https://doi.org/10.1130/GES00852.1>.
- Benowitz, J.A., Layer, P., Armstrong, P., Perry, S., Haeussler, P., Fitzgerald, P., and VanLaningham, S., 2011, Spatial variations in focused exhumation along a continental-scale strike-slip fault: The Denali fault of the eastern Alaska Range: *Geosphere*, v. 7, no. 2, p. 455–467, <https://doi.org/10.1130/GES00589.1>.
- Benowitz, J.A., Haeussler, P.J., Layer, P.W., O'Sullivan, P.B., Wallace, W.K., and Gillis, R.J., 2012a, Cenozoic tectono-thermal history of the Tordrillo Mountains, Alaska: Paleocene–Eocene ridge subduction, decreasing relief, and late Neogene faulting: *Geochemistry, Geophysics, Geosystems*, v. 13, no. 4, <https://doi.org/10.1029/2011GC003951>.
- Benowitz, J., Vansant, G., Roeske, S., Layer, P.W., Hults, C.P., and O'Sullivan, P., 2012b, Geochronological constraints on the Eocene to Present slip rate history of the eastern Denali fault system: *Geological Society of America Abstracts with Programs*, v. 44, no. 7, p. 634.
- Benowitz, J.A., Layer, P.W., and VanLaningham, S., 2014, Persistent long-term (c. 24 Ma) exhumation in the Eastern Alaska Range constrained by stacked thermochronology, *in* Jourdan, F., Mark, D.F., and Verati, C., eds., *Advances in ⁴⁰Ar/³⁹Ar Dating: From Archaeology to Planetary Sciences*: Geological Society of London Special Publication 378, p. 225–243, <https://doi.org/10.1144/SP378.12>.
- Benowitz, J.A., Davis, K., and Roeske, S., 2019, A river runs through it both ways across time: ⁴⁰Ar/³⁹Ar detrital and bedrock muscovite geochronology constraints on the Neogene paleodrainage history of the Nenana River system, Alaska Range: *Geosphere*, v. 15, no. 3, p. 682–701, <https://doi.org/10.1130/GES01673.1>.
- Berger, A.L., Spotila, J.A., Chapman, J.B., Pavlis, T.L., Enkelmann, E., Ruppert, N.A., and Buscher, J.T., 2008a, Architecture, kinematics, and exhumation of a convergent orogenic wedge: A thermochronological investigation of tectonic-climatic interactions within the central St. Elias orogen, Alaska: *Earth and Planetary Science Letters*, v. 270, p. 13–24, <https://doi.org/10.1016/j.epsl.2008.02.034>.
- Berger, A.L., Gulick, S.P.S., Spotila, J.A., Upton, P., Jaeger, J.M., Chapman, J.B., Worthington, L.A., Pavlis, T.L., Ridgway, K.D., Willems, B.A., and McAleer, R.J., 2008b, Quaternary tectonic response to intensified glacial erosion in an orogenic wedge: *Nature Geoscience*, v. 1, p. 793–799, <https://doi.org/10.1038/ngeo334>.
- Berkelhammer, S.E., 2017, Initiation of the Wrangell arc: A record of tectonic changes in an arc-transform junction revealed by new geochemistry and geochronology of the ~29–18 Ma Sonya Creek volcanic field, Alaska [M.S. thesis]: Manhattan, Kansas, Kansas State University, <http://krex.k-state.edu/dspace/handle/2097/36236>.
- Borg, L.E., Clyne, M.A., and Bullen, T.D., 1997, The variable role of slab-derived fluids in the generation of a suite of primitive calc-alkaline lavas from the southernmost Cascades, California: *Canadian Mineralogist*, v. 35, p. 425–452.
- Broussard, D.R., Trop, J.M., Benowitz, J.A., Daeschler, E.B., Chamberlain, J.A., Jr., and Chamberlain, R.B., 2018, Depositional setting, taphonomy and geochronology of new fossil sites in the Catskill Formation (Upper Devonian) of north-central Pennsylvania, USA, including a new early tetrapod fossil: *Palaeogeography, Palaeoclimatology, Palaeoecology*, v. 511, p. 168–187, <https://doi.org/10.1016/j.palaeo.2018.07.033>.
- Brueseke, M.E., and Hart, W.K., 2008, Geology and petrology of the mid-Miocene Santa Rosa-Calico volcanic field, northern Nevada: Nevada Bureau of Mines and Geology Bulletin 113, 46 p.
- Brueseke, M.E., Benowitz, J.A., Trop, J.M., Davis, K.D., Berkelhammer, P.W., Layer, P.W., and Morter, B.K., 2019, The Alaska Wrangell Arc: ~30 Ma of subduction-related magmatism along a still active arc-transform junction: *Terra Nova*, v. 31, p. 59–66, <https://doi.org/10.1111/ter.12369>.
- Castillo, P.R., 2012, Adakite petrogenesis: *Lithos*, v. 134–135, p. 304–316, <https://doi.org/10.1016/j.lithos.2011.09.013>.
- Clague, J.J., Evans, S.G., Rampton, V.N., and Woodsworth, G.J., 1995, Improved age estimates for the White River and Bridge River tephra, western Canada: *Canadian Journal of Earth Sciences*, v. 32, p. 1172–1179, <https://doi.org/10.1139/e95-096>.
- Cobbett, R., Israel, S., Mortenson, J., Joyce, N., and Crowley, J., 2017, Structure and kinematic evolution of the Duke River fault, southwestern Yukon: *Canadian Journal of Earth Sciences*, v. 54, p. 322–344, <https://doi.org/10.1139/cjes-2016-0074>.
- Cole, J.W., 1990, Structural control and origin of volcanism in the Taupo volcanic zone, New Zealand: *Bulletin of Volcanology*, v. 52, p. 445–459, <https://doi.org/10.1007/BF00268925>.
- Cole, R.B., and Basu, A.R., 1992, Middle Tertiary volcanism during ridge-trench interactions in western California: *Science*, v. 258, p. 793–796, <https://doi.org/10.1126/science.258.5083.793>.
- Cole, R.B., and Basu, A.R., 1995, Nd-Sr isotopic geochemistry and tectonics of ridge subduction and middle Cenozoic volcanism in western California: *Geological Society of America Bulletin*, v. 107, p. 167–179, [https://doi.org/10.1130/0016-7606\(1995\)107<0167:NSIGAT>2.3.CO;2](https://doi.org/10.1130/0016-7606(1995)107<0167:NSIGAT>2.3.CO;2).
- Cross, T.A., and Pilger, R.E., Jr., 1982, Controls of subduction geometry, location of magmatic arcs, and tectonics of arc: *Geological Society of America Bulletin*, v. 93, p. 545–562, [https://doi.org/10.1130/0016-7606\(1982\)93<545](https://doi.org/10.1130/0016-7606(1982)93<545).
- Davis, K.N., Benowitz, J., Layer, P.W., Trop, J., and Brueseke, M., 2017, Dating the lost arc of Alaska: Constraining the timing of initiation of the Wrangell arc with a new ⁴⁰Ar/³⁹Ar detrital geochronology approach on modern river lithic grains: *Geological Society of America Abstracts with Programs*, v. 49, no. 4, <https://doi.org/10.1130/abs/2017AM-296490>.
- Defant, M.J., and Drummond, M.S., 1990, Derivation of some modern arc magmas by melting of young subducted lithosphere: *Nature*, v. 347, p. 662–665, <https://doi.org/10.1038/347662a0>.
- Defant, M.J., Richerson, M., De Boer, J.Z., Stewart, R.H., Maury, R.C., Bellon, H., Drummond, M.S., Feigenson, M.D., and Jackson, T.E., 1991, Dacite genesis via both slab melting and differentiation: Petrogenesis of La Yeguada volcanic complex, Panama: *Journal of Petrology*, v. 32, p. 1101–1142, <https://doi.org/10.1093/petrology/32.6.1101>.
- Dodds, C.J., and Campbell, R.B., 1988, Potassium-argon ages of mainly intrusive rocks in the St. Elias Mountains, Yukon and British Columbia: *Geological Survey of Canada Paper 87-16*, 43 p., <https://doi.org/10.4095/126100>.
- Drake, M.J., 1975, The oxidation state of europium as an indicator of oxygen fugacity: *Geochimica et Cosmochimica Acta*, v. 39, p. 55–64, [https://doi.org/10.1016/0016-7037\(75\)90184-2](https://doi.org/10.1016/0016-7037(75)90184-2).
- Drake, M.J., and Weill, D.F., 1975, Partition of Sr, Ba, Ca, Y, Eu²⁺, Eu³⁺, and other REE between plagioclase feldspar and magmatic liquid: An experimental study: *Geochimica et Cosmochimica Acta*, v. 39, p. 689–712, [https://doi.org/10.1016/0016-7037\(75\)90011-3](https://doi.org/10.1016/0016-7037(75)90011-3).
- Drummond, M.S., Defant, M.J., and Kepezhinskas, P.K., 1996, Petrogenesis of slab-derived trondhjemite-tonalite-dacite/adakite magmas: *Royal Society of Edinburgh Transactions: Earth Science*, v. 87, p. 205–215, <https://doi.org/10.1017/S0263593300006611>.
- Dunn, C.A., Enkelmann, E., Ridgway, K.D., and Allen, W.K., 2017, Source to sink evaluation of sediment routing in the Gulf of Alaska and Southeast Alaska: A thermochronometric perspective: *Journal of Geophysical Research: Earth Surface*, v. 122, p. 711–734, <https://doi.org/10.1002/2016JF004168>.
- Eberhart-Phillips, D., et al., 2003, The 2002 Denali fault earthquake, Alaska: A large magnitude, slip-partitioned event: *Science*, v. 300, p. 1113–1118, <https://doi.org/10.1126/science.1082703>.
- Eberhart-Phillips, D., Christensen, D.H., Brocher, T.M., Hansen, R., Ruppert, N.A., Haeussler, P.J., and Abers, G.A., 2006, Imaging the transition from Aleutian subduction to Yakutat collision in central Alaska with local earthquakes and active source data: *Journal of Geophysical Research*, v. 111, <https://doi.org/10.1029/2005JB004240>.
- Edwards, B.R., and Russell, J.K., 2000, Distribution, nature, and origin of Neogene–Quaternary magmatism in the northern Cordilleran volcanic province, Canada: *Geological Society of America Bulletin*, v. 112, p. 1280–1295, [https://doi.org/10.1130/0016-7606\(2000\)112<1280:DNAOON>2.0.CO;2](https://doi.org/10.1130/0016-7606(2000)112<1280:DNAOON>2.0.CO;2).
- Eiché, G.E., Francis, D.M., and Ludden, J.N., 1987, Primary alkaline magmas associated with the Quaternary Alligator Lake volcanic complex, Yukon Territory, Canada: *Contributions to Mineralogy and Petrology*, v. 95, p. 191–201, <https://doi.org/10.1007/BF00381268>.
- Engelbreton, D.C., Cox, A., and Gordon, R.G., 1985, Relative Motions between Oceanic and Continental Plates in the Pacific Basin: *Geological Society of America Special Paper 206*, 59 p., <https://doi.org/10.1130/SPE206-p1>.
- England, P.C., and Katz, R.F., 2010, Melting above the anhydrous solidus controls the location of volcanic arcs: *Nature*, v. 467, p. 700–703, <https://doi.org/10.1038/nature09417>.

- Enkelmann, E., Garver, J.I., and Pavlis, T.L., 2008, Rapid exhumation of ice-covered rocks of the Chugach–St. Elias orogen, southeast Alaska: *Geology*, v. 36, p. 915–918, <https://doi.org/10.1130/G2252A.1>.
- Enkelmann, E., Zeitler, P.K., Garver, J.I., Pavlis, T.L., and Hooks, B.P., 2010, The thermochronological record of tectonic and surface process interaction at the Yakutat–North American collision zone in southeast Alaska: *American Journal of Science*, v. 310, p. 231–260, <https://doi.org/10.2475/04.2010.01>.
- Enkelmann, E., Piastreniewicz, A., Falkowski, S., Stübner, K., and Ehlers, T.A., 2017, Thermochronology in southeast Alaska and southwest Yukon: Implications for North American Plate response to terrane accretion: *Earth and Planetary Science Letters*, v. 457, p. 348–358, <https://doi.org/10.1016/j.epsl.2016.10.032>.
- Falkowski, S., and Enkelmann, E., 2016, Upper-crustal cooling of the Wrangellia composite terrane in the northern St. Elias Mountains, western Canada: *Lithosphere*, v. 8, p. 359–378, <https://doi.org/10.1130/L508.1>.
- Falkowski, S., Enkelmann, E., and Ehlers, T., 2014, Constraining the area of rapid and deep-seated exhumation at the St. Elias syntaxis, southeast Alaska, with detrital zircon fission-track analysis: *Tectonics*, v. 33, p. 597–616, <https://doi.org/10.1002/2013TC003408>.
- Falkowski, S., Enkelmann, E., Drost, K., Pfänder, J., Stübner, K., and Ehlers, T.A., 2016, Cooling history of the St. Elias syntaxis, southeast Alaska, revealed by geochronology and thermochronology of cobble-sized glacial detritus: *Tectonics*, v. 35, p. 447–468.
- Ferrari, L., Petrone, C.M., and Francalanci, L., 2001, Generation of oceanic-island basalt-type volcanism in the western Trans-Mexican volcanic belt by slab rollback, asthenosphere infiltration, and variable flux melting: *Geology*, v. 29, p. 507–510, [https://doi.org/10.1130/0091-7613\(2001\)029<0507:GOOIBT>2.0.CO;2](https://doi.org/10.1130/0091-7613(2001)029<0507:GOOIBT>2.0.CO;2).
- Ferris, A., Abers, G.A., Christensen, D.H., and Veenstra, E., 2003, High resolution image of the subducted Pacific plate beneath central Alaska, 50–150 km depth: *Earth and Planetary Science Letters*, v. 214, p. 575–588, [https://doi.org/10.1016/S0012-821X\(03\)00403-5](https://doi.org/10.1016/S0012-821X(03)00403-5).
- Finzel, E.S., Trop, J.M., Ridgway, K.D., and Enkelmann, E., 2011, Upper plate proxies for flat-slab subduction processes in southern Alaska: *Earth and Planetary Science Letters*, v. 303, p. 348–360, <https://doi.org/10.1016/j.epsl.2011.01.014>.
- Finzel, E.S., Enkelmann, E., Falkowski, S., and Hedeon, T., 2016, Long-term fore-arc basin evolution in response to changing subduction styles in southern Alaska: *Tectonics*, v. 35, p. 1735–1759, <https://doi.org/10.1002/2016TC004171>.
- Frost, B.R., and Frost, C.D., 2008, A geochemical classification for feldspathic igneous rocks: *Journal of Petrology*, v. 49, p. 1955–1969, <https://doi.org/10.1093/petrology/egn054>.
- Gaschnig, R.M., Vervoort, J.D., Lewis, R.S., and Tikoff, B., 2011, Isotopic evolution of the Idaho Batholith and Challis intrusive province, northern US Cordillera: *Journal of Petrology*, v. 52, no. 12, p. 2397–2429.
- Gill, J.B., 1981, *Orogenic Andesite and Plate Tectonics*: Berlin, Heidelberg, Springer-Verlag, 390 p., <https://doi.org/10.1007/978-3-642-68012-0>.
- Gill, R., 2010, *Igneous Rocks and Processes: A Practical Guide*: West Sussex, UK, Wiley-Blackwell, 428 p.
- Grabowski, D.M., Enkelmann, E., and Ehlers, T.A., 2013, Spatial extent of rapid denudation in the glaciated St. Elias syntaxis region, SE Alaska: *Journal of Geophysical Research. Earth Surface*, v. 118, p. 1921–1938, <https://doi.org/10.1002/jgrf.20136>.
- Greene, A.R., Scoates, J.S., and Weis, D., 2008, Wrangellia flood basalts in Alaska: A record of plume-lithosphere interaction in a Late Triassic accreted oceanic plateau: *Geochemistry, Geophysics, Geosystems*, v. 9, no. 12, <https://doi.org/10.1029/2008GC002092>.
- Greene, A.R., Scoates, J.S., Weis, D., and Israel, S., 2009, Geochemistry of Triassic flood basalts from the Yukon (Canada) segment of the accreted Wrangellia oceanic plateau: *Lithos*, v. 110, p. 1–19, <https://doi.org/10.1016/j.lithos.2008.11.010>.
- Grove, T.L., Elkins-Tanton, L.T., Parman, S.W., Chatterjee, N., Muntener, O., and Gaetani, G.A., 2003, Fractional crystallization and mantle-melting controls on calc-alkaline differentiation trends: *Contributions to Mineralogy and Petrology*, v. 145, p. 515–533, <https://doi.org/10.1007/s00410-003-0448-z>.
- Grove, T.L., Till, C.B., and Krawczynski, M.J., 2012, The role of H₂O in subduction zone magmatism: *Annual Review of Earth and Planetary Sciences*, v. 40, p. 413–439, <https://doi.org/10.1146/annurev-earth-042711-105310>.
- Gulick, S.P., Reece, R.S., Christeson, G.L., Van Avendonk, H., Worthington, L.L., and Pavlis, T.L., 2013, Seismic images of the Transition fault and the unstable Yakutat–Pacific–North American triple junction: *Geology*, v. 41, p. 571–574, <https://doi.org/10.1130/G33900.1>.
- Gutscher, M.-A., Maury, R., Eissen, J.-P., and Bourdon, E., 2000, Can slab melting be caused by flat subduction?: *Geology*, v. 28, p. 535–538, [https://doi.org/10.1130/0091-7613\(2000\)28<535:CSMBCB>2.0.CO;2](https://doi.org/10.1130/0091-7613(2000)28<535:CSMBCB>2.0.CO;2).
- Haessler, P.J., 2008, An overview of the neotectonics of interior Alaska: Far-field deformation from the Yakutat microplate collision, in Freymueller, J.T., et al., eds., *Active Tectonics and Seismic Potential of Alaska*: American Geophysical Union Geophysical Monograph 179, p. 83–108, <https://doi.org/10.1029/179GM05>.
- Haessler, P.J., Matmon, A., Schwartz, D.P., and Seits, G.G., 2017, Neotectonics of interior Alaska and the late Quaternary slip rate along the Denali fault system: *Geosphere*, v. 13, p. 1445–1463, <https://doi.org/10.1130/GES01447.1>.
- Irvine, T.N., and Baragar, W.R.A., 1971, A guide to the chemical classification of the common volcanic rocks: *Canadian Journal of Earth Sciences*, v. 8, p. 523–548, <https://doi.org/10.1139/e71-055>.
- Irving, A.J., and Frey, F.A., 1984, Trace element abundances in megacrysts and their host basalts: Constraints on partition coefficients and megacryst genesis: *Geochimica et Cosmochimica Acta*, v. 48, p. 1201–1221, [https://doi.org/10.1016/0016-7037\(84\)90056-5](https://doi.org/10.1016/0016-7037(84)90056-5).
- Jadamec, M., and Billen, M.I., 2012, The role of rheology and slab shape on rapid mantle flow: Three-dimensional numerical models of the Alaska slab edge: *Journal of Geophysical Research*, v. 117, B02304, <https://doi.org/10.1029/2011JB008563>.
- Jadamec, M.A., 2016, Insights on slab-driven mantle flow from advances in three-dimensional modeling: *Journal of Geodynamics*, v. 100, p. 51–70, <https://doi.org/10.1016/j.jog.2016.07.004>.
- Jadamec, M.A., and Billen, M.I., 2010, Reconciling surface plate motions with rapid three-dimensional mantle flow around a slab edge: *Nature*, v. 465, p. 338–341, <https://doi.org/10.1038/nature09053>.
- Jicha, B.R., Garcia, M.O., Wessel, P., 2018, Mid-Cenozoic Pacific plate motion change: Implications for the northwest Hawaiian Ridge and circum-Pacific: *Geology*, v. 46, p. 939–942, <https://doi.org/10.1130/G45175.1>.
- Johnson, D.M., Hooper, P.R., and Conrey, R.M., 1999, XRF analysis of rocks and minerals for major and trace elements on a single low dilution Li-tetraborate fused bead: *Advances in X-Ray Analysis*, v. 41, p. 843–867.
- Kalbas, J.L., Ridgway, K.D., and Gehrels, G.E., 2008, Stratigraphy, depositional systems, and provenance of the Lower Cretaceous Kahiltna assemblage, western Alaska Range: Basin development in response to oblique collision, in Ridgway, K.D., Trop, J.M., O'Neill, J.M., and Glen, J.M.G., eds., *Tectonic Growth of a Collisional Continental Margin: Crustal Evolution of Southern Alaska*: Geological Society of America Special Paper 431, p. 307–344.
- Karsli, O., Ketenci, M., Uysal, I., Dokuz, A., Aydin, F., Chen, B., Kandemir, R., and Wijbrans, J., 2011, Adakite-like granitoid porphyries in the Eastern Pontides, NE Turkey: Potential parental melts and geodynamic implications: *Lithos*, v. 127, p. 354–372, <https://doi.org/10.1016/j.lithos.2011.08.014>.
- Kelemen, P.B., Yogodzinski, G.M., and Scholl, D.W., 2003, Along strike variation in the Aleutian Island arc: Genesis of high Mg# andesite and implications for continental crust, in Eiler, J., ed., *The Subduction Factory*: American Geophysical Union, Geophysical Monograph Series, v. 138, p. 223–276, <https://doi.org/10.1029/138GM11>.
- Kepezhinskas, P.K., Defant, M.J., and Drummond, M.S., 1995, Na metasomatism in the island-arc mantle by slab melt–Peridotite interaction: Evidence from mantle xenoliths in the north Kamchatka arc: *Journal of Petrology*, v. 36, no. 6, p. 1505–1527, <https://doi.org/10.1093/oxfordjournals.petrology.a037263>.
- Layer, P.W., Hall, C.M., and York, D., 1987, The derivation of ⁴⁰Ar/³⁹Ar age spectra of single grains of hornblende and biotite by laser step heating: *Geophysical Research Letters*, v. 14, p. 757–760, <https://doi.org/10.1029/GL014i007p00757>.
- Lease, R., Haessler, P.J., and O'Sullivan, P., 2016, Changing exhumation patterns during Cenozoic growth and glaciation of the Alaska Range: Insight from detrital geo- and thermo-chronology: *Tectonics*, v. 35, p. 934–955, <https://doi.org/10.1002/2015TC004067>.
- Le Bas, M.J., Le Maitre, R.W., Streckeisen, A., and Zanettin, B.A., 1986, Chemical classification of volcanic rocks based on the total alkali-silica diagram: *Journal of Petrology*, v. 27, p. 745–750, <https://doi.org/10.1093/petrology/27.3.745>.
- Lee, H.Y., Chung, S.L., and Yang, H.M., 2016, Late Cenozoic volcanism in central Myanmar: Geochemical characteristics and geodynamic significance: *Lithos*, v. 245, p. 174–190, <https://doi.org/10.1016/j.lithos.2015.09.018>.
- Le Maitre, R.W., 1976, Some problems of the projection of chemical data into mineralogical classifications: *Contributions to Mineralogy and Petrology*, v. 56, no. 2, p. 181–189, <https://doi.org/10.1007/BF00399603>.

- Luhr, J., 2000, The geology and petrology of Volcán San Juan (Nayarit, México) and the compositionally zoned Tepic Pumice: *Journal of Volcanology and Geothermal Research*, v. 95, p. 109–156, [https://doi.org/10.1016/S0377-0273\(99\)00133-X](https://doi.org/10.1016/S0377-0273(99)00133-X).
- Lunt, A.S., 1997, A reconnaissance study of mafic to intermediate intra-arc volcanism in the western Wrangell Volcanic Field, Alaska [M.S. thesis]: Oxford, Ohio, Miami University, 150 p.
- Marechal, A., Ritz, J.-F., Ferry, M., Mazzotti, S., Blard, P.-H., Braucher, R., and Saint-Carlier, D., 2018, Active tectonics around the Yakutat indenter: New geomorphological constraints on the eastern Denali, Totschunda and Duke River Faults: *Earth and Planetary Science Letters*, v. 482, p. 71–80, <https://doi.org/10.1016/j.epsl.2017.10.051>.
- Martin-Short, R., Allen, R.M., and Bastow, I.D., 2016, Subduction geometry beneath south-central Alaska and its relationship to volcanism: *Geophysical Research Letters*, v. 43, p. 9509–9517, <https://doi.org/10.1002/2016GL070580>.
- Martin-Short, R., Allen, R., Bastow, I.D., Porritt, R.W., and Miller, M.S., 2018, Seismic imaging of the Alaska subduction zone: Implications for slab geometry and volcanism: *Geochemistry, Geophysics, Geosystems*, v. 19, no. 11, p. 4541–4560, <https://doi.org/10.1029/2018GC007962>.
- Matmon, A., Schwartz, D.P., Haeussler, P.J., Finkel, R., Kienkaemper, J.J., Stenner, H.D., and Dawson, T.E., 2006, Denali fault slip rates and Holocene–late Pleistocene kinematics of central Alaska: *Geology*, v. 34, p. 645–648, <https://doi.org/10.1130/G22361.1>.
- Mauri, R.C., Pubellier, M., Rangin, C., Wulput, L., Cotton, J., Socquet, A., Bellon, H., Gullaud, J.P., and Htun, H.M., 2004, Quaternary calc-alkaline and alkaline volcanism in a hyper-oblique convergence setting, central Myanmar and western Yunnan: *Bulletin de la Société Géologique de France*, v. 175, p. 461–472, <https://doi.org/10.2113/175.5.461>.
- McAleer, R.J., Spotila, J.A., Enkelmann, E., and Berger, A.L., 2009, Exhumation along the Fairweather fault, southeast Alaska, based on low-temperature thermochronometry: *Tectonics*, v. 28, TC1007, <https://doi.org/10.1029/2007TC002240>.
- McDougall, I., and Harrison, T.M., 1999, *Geochronology and Thermochronology by the ⁴⁰Ar/³⁹Ar Method* (2nd edition): New York, Oxford University Press, 269 p.
- McGeary, S., Nur, A., and Ben-Avraham, Z., 1985, Spatial gaps in arc volcanism: The effect of collision or subduction of oceanic plateaus: *Tectonophysics*, v. 119, p. 195–221, [https://doi.org/10.1016/0040-1951\(85\)90039-3](https://doi.org/10.1016/0040-1951(85)90039-3).
- McNamara, D.E., and Pasyanos, M.E., 2002, Seismological evidence for a sub-volcanic arc mantle wedge beneath the Denali volcanic gap, Alaska: *Geophysical Research Letters*, v. 29, no. 16, p. 61–1–61–4, <https://doi.org/10.1029/2001GL014088>.
- Mertzman, S.A., 2000, K-Ar results from the southern Oregon–northern California Cascade Range: *Oregon Geology*, v. 62, p. 99–122.
- Mertzman, S.A., 2015, XRF laboratory: Overview and analytical procedures: <http://www.fandm.edu/earth-environment/laboratory-facilities/instrument-use-and-instructions> (accessed 15 April 2017).
- Miyashiro, A., 1974, Volcanic rock series in island arcs and active continental margins: *American Journal of Science*, v. 274, p. 321–355, <https://doi.org/10.2475/ajs.274.4.321>.
- Morter, B.K., Brueske, M.E., Benowitz, J.A., Trop, J.M., Davis, K., and Layer, P.W., 2016, Linking geochemistry of Cenozoic volcanic clasts from the Wrangell Arc, Alaska, to upper plate and subducting slab tectonic processes: *Geological Society of America Abstracts with Programs*, v. 48, no. 7, <https://doi.org/10.1130/abs/2016AM-278622>.
- Nokleberg, W.J., Plafker, G., and Wilson, F.H., 1994, Geology of southcentral Alaska, in Plafker, G., and Berg, H.C., eds., *The Geology of Alaska: Boulder, Colorado, Geological Society of America, Geology of North America*, v. G-1, p. 311–366, <https://doi.org/10.1130/DNAG-GNA-G1.311>.
- Nye, C., Wyssm, M., Ratchkovski, N., and Fletcher, H., 2002, Magmatism in the Denali Volcanic Gap, southern Alaska: *Eos (Transactions, American Geophysical Union)*, v. 83, Abstract V12C-06.
- Nye, C.J., 1983, *Petrology and Geochemistry of Okmok and Wrangell Volcanoes, Alaska* [Ph.D. thesis]: University of California, Santa Cruz, 125 p.
- Page, R.A., Biswas, N.N., Lahr, J.C., and Hulpán, H., 1991, Seismicity of continental Alaska, in Slemmons, D.B., et al., eds., *Neotectonics of North America: Geological Society of America, Geology of North America, Decade Map Volume*, p. 47–68.
- Park, J., Levin, V., Brandon, M., Lees, J., Peyton, V., Gordeev, E., and Ozerov, A., 2002, A dangling slab, amplified arc volcanism, mantle flow and seismic anisotropy in the Kamchatka plate corner, in Stein, S., and Freymueller, J.T., eds., *Plate Boundary Zones: American Geophysical Union Geodynamics Series*, v. 30, p. 295–324, <https://doi.org/10.1029/GD030p0295>.
- Pavlis, G.L., Bauer, M.A., Elliott, J.L., Koons, P., Pavlis, T.L., Ruppert, N., Ward, K.M., and Worthington, L.L., 2019, A unified three-dimensional model of lithospheric structure at the subduction corner in southeast Alaska: Summary from STEEP: *Geosphere*, v. 15, p. 382–406, <https://doi.org/10.1130/GES01488.1>.
- Pavlis, T.L., Picornell, C., Serpa, L., Bruhn, R.L., and Plafker, G., 2004, Tectonic processes during oblique collision: Insights from the St. Elias orogen, northern North American Cordillera: *Tectonics*, v. 23, no. 3, <https://doi.org/10.1029/2003TC001557>.
- Peacock, S.M., Rushmer, T., and Thompson, A.B., 1994, Partial melting of subducting oceanic crust: *Earth and Planetary Science Letters*, v. 121, p. 227–244, [https://doi.org/10.1016/0012-821X\(94\)90042-6](https://doi.org/10.1016/0012-821X(94)90042-6).
- Pearce, J.A., and Norry, M.J., 1979, Petrogenetic implications of Ti, Zr, Y, and Nb variations in volcanic rocks: *Contributions to Mineralogy and Petrology*, v. 69, p. 33–47, <https://doi.org/10.1007/BF00375192>.
- Pearce, J.A., and Peate, D.W., 1995, Tectonic implications of the composition of volcanic arc magmas: *Annual Review of Earth and Planetary Sciences*, v. 23, p. 251–285, <https://doi.org/10.1146/annurev.earth.23.050195.001343>.
- Pearce, J.A., Harris, N.B.W., and Tindle, A.G., 1984, Trace element discrimination diagrams for the tectonic interpretation of granitic rocks: *Journal of Petrology*, v. 25, p. 956–983, <https://doi.org/10.1093/petrology/25.4.956>.
- Pearce, J.A., Stern, R.J., Bloomer, S.H., and Fryer, P., 2005, Geochemical mapping of the Mariana arc-basin system: implications for the nature and distribution of subduction components: *Geochemistry, Geophysics, Geosystems*, v. 6, no. 7, <https://doi.org/10.1029/2004GC000895>.
- Plafker, G., and Berg, H.C., 1994, Overview of the geology and tectonic evolution of Alaska, in Plafker, G., and Berg, H.C., eds., *The Geology of Alaska: Boulder, Colorado, Geological Society of America, The Geology of North America*, v. G-1, p. 989–1021, <https://doi.org/10.1130/DNAG-GNA-G1.989>.
- Portnyagin, M., and Manea, V.C., 2008, Mantle temperature control on composition of arc magmas along the Central Kamchatka Depression: *Geology*, v. 36, p. 519–522, <https://doi.org/10.1130/G24636A.1>.
- Portnyagin, M., Horenle, K., Avdeiko, G., Hauff, F., Werner, R., Bindeman, I., Uspensky, V., and Garbe-Schönberg, D., 2005, Transition from arc to oceanic magmatism at the Kamchatka-Aleutian junction: *Geology*, v. 33, p. 25–28, <https://doi.org/10.1130/G20853.1>.
- Portnyagin, M., Bindeman, I., Hoernle, K., and Hauff, F., 2007, Geochemistry of primitive lavas of the central Kamchatka depression: Magma generation at the edge of the Pacific Plate, in Eichelberger, J.A., et al., eds., *Volcanism and Subduction: The Kamchatka Region: American Geophysical Union Geophysical Monograph*, v. 172, p. 199–239, <https://doi.org/10.1029/172GM16>.
- Preece, S.J., and Hart, W.K., 2004, Geochemical variations in the <5 Ma Wrangell Volcanic Field, Alaska: Implications for the magmatic and tectonic development of a complex continental arc system: *Tectonophysics*, v. 392, p. 165–191, <https://doi.org/10.1016/j.tecto.2004.04.011>.
- Preece, S.J., McGimsey, R.G., Westgate, J.A., Pearce, N.J.G., Hart, W.K., and Perkins, W.T., 2014, Chemical complexity and source of the White River Ash, Alaska and Yukon: *Geosphere*, v. 10, p. 1020–1042, <https://doi.org/10.1130/GES00953.1>.
- Qi, C., Zhao, D.P., and Chen, Y., 2007, Search for deep slab segments under Alaska: Physics of the Earth and Planetary Interiors, v. 165, p. 68–82, <https://doi.org/10.1016/j.pepi.2007.08.004>.
- Rapp, R.P., Shimizu, N., Norman, M.D., and Applegate, G.S., 1999, Reaction between slab-derived melts and peridotite in the mantle wedge: Experimental constraints at 3.8 GPa: *Chemical Geology*, v. 160, p. 335–356, [https://doi.org/10.1016/S0009-2541\(99\)00106-0](https://doi.org/10.1016/S0009-2541(99)00106-0).
- Renne, P.R., Mundil, R., Balco, G., Min, K., and Ludwig, K.R., 2010, Joint determination of ⁴⁰K decay constants and ⁴⁰Ar/³⁹Ar for the Fish Canyon sanidine standard, and improved accuracy for ⁴⁰Ar/³⁹Ar geochronology: *Geochimica et Cosmochimica Acta*, v. 74, p. 5349, <https://doi.org/10.1016/j.gca.2010.06.017>.
- Richter, D.H., 1976, Geologic map of the Nabesna quadrangle, Alaska: U.S. Geological Survey Miscellaneous Geological Investigations Series Map I-932, scale 1: 250,000.
- Richter, D.H., and Matson, J.A., 1971, Quaternary faulting in the eastern Alaska Range: *Geological Society of America Bulletin*, v. 82, p. 1529–1540, [https://doi.org/10.1130/0016-7606\(1971\)82\[1529:QFITEA\]2.0.CO;2](https://doi.org/10.1130/0016-7606(1971)82[1529:QFITEA]2.0.CO;2).
- Richter, D.H., Smith, J.G., Lanphere, M.A., Dalrymple, G.B., Reed, B.L., and Shew, N., 1990, Age and progression of volcanism, Wrangell volcanic field, Alaska: *Bulletin of Volcanology*, v. 53, p. 29–44, <https://doi.org/10.1007/BF00680318>.
- Richter, D.H., Ratté, J.C., Leeman, W.P., and Menzies, M., 2000, Geologic map of the McCarthy D-1 quadrangle, Alaska: U.S. Geological Survey Geologic Investigations Series I-2695, scale 1: 63,360.
- Ridgway, K.D., and DeCelles, P.G., 1993, Stream-dominated alluvial-fan and lacustrine depositional systems in Cenozoic strike-slip basins, Denali fault system, Yukon Territory, Canada: *Sedimentology*, v. 40, p. 645–666, <https://doi.org/10.1111/j.1365-3091.1993.tb01354.x>.

- Ridgway, K.D., Trop, J.M., and Finzel, E.S., 2012, Modification of continental forearc basins by flat-slab subduction processes: A case study from southern Alaska, *in* Busby, C., and Azor, A., eds., *Tectonics of Sedimentary Basins: Recent Advances*: John Wiley and Sons, Inc., Wiley Online Library, p. 327–346, <https://doi.org/10.1002/9781444347166.ch16>.
- Roddick, J.C., 1978, The application of isochron diagrams in $^{40}\text{Ar}/^{39}\text{Ar}$ dating: A discussion: *Earth and Planetary Science Letters*, v. 41, p. 233–244, [https://doi.org/10.1016/0012-821X\(78\)90014-6](https://doi.org/10.1016/0012-821X(78)90014-6).
- Roddick, J.C., Cliff, R.A., and Rex, D.C., 1980, The evolution of excess argon in alpine biotites—A $^{40}\text{Ar}/^{39}\text{Ar}$ analysis: *Earth and Planetary Science Letters*, v. 48, p. 185–208, [https://doi.org/10.1016/0012-821X\(80\)90181-8](https://doi.org/10.1016/0012-821X(80)90181-8).
- Rudnick, R.L., and Gao, S., 2003, Composition of the Continental Crust, *in* Holland, H.D., and Turekian, K.K., eds., *The Crust: Treatise on Geochemistry*, v. 3, p. 1–64.
- Sajona, F.G., Maury, R.C., Bellond, H., Cotten, J., Defant, M.J., and Pubellier, M., 1993, Initiation of subduction and the generation of slab melts in western and eastern Mindanao, Philippines: *Geology*, v. 21, p. 1007–1010, [https://doi.org/10.1130/0091-7613\(1993\)021<1007:IOSATG>2.3.CO;2](https://doi.org/10.1130/0091-7613(1993)021<1007:IOSATG>2.3.CO;2).
- Skulski, T., Francis, D., and Ludden, J., 1991, Arc-transform magmatism in the Wrangell volcanic belt: *Geology*, v. 19, p. 11–14, [https://doi.org/10.1130/0091-7613\(1991\)019<0011:ATMITW>2.3.CO;2](https://doi.org/10.1130/0091-7613(1991)019<0011:ATMITW>2.3.CO;2).
- Skulski, T., Francis, D., and Ludden, J., 1992, Volcanism in an arc-transform transition zone: the stratigraphy of the St. Clare Creek volcanic field, Wrangell volcanic belt, Yukon, Canada: *Canadian Journal of Earth Sciences*, v. 29, p. 446–461, <https://doi.org/10.1139/e92-039>.
- Stern, C.R., and Kilian, R., 1996, Role of the subducted slab, mantle wedge and continental crust in the generation of adakites from the Austral Volcanic Zone: *Contributions to Mineralogy and Petrology*, v. 123, no. 3, p. 263–281, <https://doi.org/10.1007/s004100050155>.
- Stern, R.J., 2002, Subduction Zones: Reviews of Geophysics, v. 40, p. 1012, <https://doi.org/10.1029/2001RG000108>.
- Streck, M.J., and Leeman, W.P., 2018, Petrology of “Mt. Shasta” high-magnesian andesite (HMA): A product of multi-stage crustal assembly: *The American Mineralogist*, v. 103, p. 216–240, <https://doi.org/10.2138/am-2018-6151>.
- Sun, S.S., and McDonough, W.F., 1989, Chemical and isotopic systematics of oceanic basalts: implications for mantle composition and processes: *Geological Society of London Special Publications*, v. 42, p. 313–345, <https://doi.org/10.1144/GSL.SP.1989.042.01.19>.
- Sun, W.D., Hu, Y.H., Kamenetsky, V.S., Eggins, S.M., Chen, M., and Arculus, R.J., 2008, Constancy of Nb/U in the mantle revisited: *Geochimica et Cosmochimica Acta*, v. 72, p. 3542–3549, <https://doi.org/10.1016/j.gca.2008.04.029>.
- Syracuse, E.M., and Abers, G.A., 2006, Global compilation of variations in slab depth beneath arc volcanoes and implications: *Geochemistry, Geophysics, Geosystems*, v. 7, no. 5, <https://doi.org/10.1029/2005GC001045>.
- Takada, A., 1994, The influence of regional stress and magmatic input on styles of monogenetic and polygenetic volcanism: *Journal of Geophysical Research*, v. 99, p. 13,563–13,573, <https://doi.org/10.1029/94JB00494>.
- Thorkelson, D.J., Madsen, J.K., and Slugget, C.L., 2011, Mantle flow through the Northern Cordilleran slab window revealed by volcanic geochemistry: *Geology*, v. 39, p. 267–270, <https://doi.org/10.1130/G31522.1>.
- Tibaldi, A., Pasquare, F., and Tormey, D., 2010, Volcanism in reverse and strike-slip fault settings, *in* Cloetingh, S., and Negendank, J., eds., *New Frontiers in Integrated Solid Earth Sciences*: Dordrecht, The Netherlands, Springer-Verlag, p. 315–348.
- Trop, J.M., Hart, W.K., Snyder, D.C., and Idleman, B., 2012, Miocene basin development and volcanism along a strike-slip to flat-slab subduction transition: Stratigraphy, geochemistry, and geochronology of the central Wrangell volcanic belt, Yakutat–North America collision zone: *Geosphere*, v. 8, p. 805–834, <https://doi.org/10.1130/GES00762.1>.
- Trop, J.M., Benowitz, J.A., Brueseke, M.E., Layer, P.W., Kirby, C.S., Davis, K.N., Berkelhammer, S.E., and Morter, B.K., 2018, Geochronologic constraints on ~30 million years of diachronous magmatism along an arc-transform junction, Wrangell Arc, southern Alaska and Canada: *Geological Society of America Abstracts with Programs*, v. 50, no. 6, <https://doi.org/10.1130/abs/2018AM-316750>.
- Trop, J.M., Benowitz, J.A., Cole, R., and O’Sullivan, P., 2019, Cretaceous to Miocene magmatism, sedimentation, and exhumation within the Alaska Range suture zone: A polyphaser reactivated terrane boundary: *Geosphere*, v. 15, <https://doi.org/10.1130/GES02014.1>.
- van Hunen, J., van den Berg, A., and Vlaar, N., 2002, On the role of subducting oceanic plateaus in the development of shallow flat subduction: *Tectonophysics*, v. 352, p. 317–333, [https://doi.org/10.1016/S0040-1951\(02\)00263-9](https://doi.org/10.1016/S0040-1951(02)00263-9).
- Vaughan, A.P.M., and Scarrow, J.H., 2003, K-rich mantle metasomatism control of localization and initiation of lithospheric strike-slip faulting: *Terra Nova*, v. 15, p. 163–169, <https://doi.org/10.1046/j.1365-3121.2003.00485.x>.
- Venereau, C.M., Martin-Short, R., Bastow, I.D., Allen, R.M., and Kounoudis, R., 2019, The role of variable slab dip in driving mantle flow at the eastern edge of the Alaskan subduction margin: Insights from SKS shear-wave splitting: *Geochemistry, Geophysics, Geosystems*, <https://doi.org/10.1029/2018GC008170>.
- Waldien, T.S., Roeske, S.M., Benowitz, J.A., Allen, W.K., Ridgway, K.D., and O’Sullivan, P.B., 2018, Late Miocene to Quaternary evolution of the McCallum Creek thrust system, Alaska: Insights for range-boundary thrusts in transpressional orogens: *Geosphere*, v. 14, p. 2379–2406, <https://doi.org/10.1130/GES01676.1>.
- Wang, Q., Xu, J.F., Jian, P., Bao, Z.W., Zhao, Z.H., Li, C.F., Xiong, X.L., and Ma, J.L., 2006, Petrogenesis of adakitic porphyries in an extensional tectonic setting, Dexing, South China: Implications for the genesis of porphyry copper mineralization: *Journal of Petrology*, v. 47, p. 119–144, <https://doi.org/10.1093/petrology/egi070>.
- Weber, M.A., Brueseke, M.E., Benowitz, J.A., Trop, J.M., Berkelhammer, S.E., Davis, K.N., Layer, P.W., Morter, B.K., and Mertzman, S.A., 2017, Geological and geochemical constraints on Oligo-Miocene hypabyssal intrusive bodies from the Wrangell Arc, Alaska: *Geological Society of America Abstracts with Programs*, v. 49, no. 4, paper no. 28-3, <https://doi.org/10.1130/abs/2017CD-292655>.
- Wech, A.G., 2016, Extending Alaska’s plate boundary: Tectonic tremor generated by Yakutat subduction: *Geology*, v. 44, p. 587–590, <https://doi.org/10.1130/G37817.1>.
- Whalen, J.B., Currie, K.L., and Chappell, B.W., 1987, A-type granites: Geochemical characteristics, discrimination and petrogenesis: *Contributions to Mineralogy and Petrology*, v. 95, p. 407–419, <https://doi.org/10.1007/BF00402202>.
- Worthington, L.L., Van Avendonk, H.J.A., Gulick, S.P.S., Christeson, G.L., and Pavlis, T.L., 2012, Crustal structure of the Yakutat terrane and the evolution of subduction and collision in southern Alaska: *Journal of Geophysical Research*, v. 117, <https://doi.org/10.1029/2011JB008493>.
- Xu, J.F., Shinjio, R., Defant, M.J., Wang, Q., and Rapp, R.P., 2002, Origin of Mesozoic adakitic intrusive rocks in the Ningzhen area of east China: Partial melting of delaminated lower continental crust?: *Geology*, v. 30, p. 1111–1114, [https://doi.org/10.1130/0091-7613\(2002\)030<1111:OOMAIR>2.0.CO;2](https://doi.org/10.1130/0091-7613(2002)030<1111:OOMAIR>2.0.CO;2).
- Yogodzinski, G.M., Kay, R.W., Volynets, O.N., Koloskov, A.V., and Kay, S.M., 1995, Magnesian andesite in the western Aleutian Komandorsky region: Implications for slab melting and processes in the mantle wedge: *Geological Society of America Bulletin*, v. 107, p. 505–519, [https://doi.org/10.1130/0016-7606\(1995\)107<0505:MAITWA>2.3.CO;2](https://doi.org/10.1130/0016-7606(1995)107<0505:MAITWA>2.3.CO;2).
- Yogodzinski, G.M., Lees, J.M., Churikova, T.G., Dorendorf, F., Wöerner, G., and Volynets, O.N., 2001, Geochemical evidence for the melting of subducting oceanic lithosphere at plate edges: *Nature*, v. 409, p. 500–504, <https://doi.org/10.1038/35054039>.
- York, D., Hall, C.M., Yanase, Y., Hanes, J.A., and Kenyon, W.J., 1981, $^{40}\text{Ar}/^{39}\text{Ar}$ dating of terrestrial minerals with a continuous laser: *Geophysical Research Letters*, v. 8, p. 1136–1138, <https://doi.org/10.1029/GL008i011p01136>.